Hydrothermal synthesis of magnetic-biochar nanocomposite derived from avocado peel and its performance as an adsorbent for the removal of methylene blue from wastewater

Eswaran Prabakaran[a], Kriveshini Pillay[b], Hendrik Brink[a*]

[a]*Department of Chemical Engineering, Water Utilisation and Environmental Engineering Division, University of Pretoria, Pretoria, South Africa.*

[b]*Department of Chemical Sciences, University of Johannesburg, Doornfontein Campus, Johannesburg, 2028, South Africa.*

Highlights

○ Magnetic Fe_3O_4-BC nanocomposite was successfully prepared by hydrothermal method.

○ TEM, FT-IR, and EDAX confirmed the successful formation of Fe_3O_4-BC.

○ Fe_3O_4-BC removes methylene blue 1–3 orders of magnitude faster than previously.

○ Fe_3O_4-BC nanocomposite was successfully regenerated at least four times.

Graphical abstract

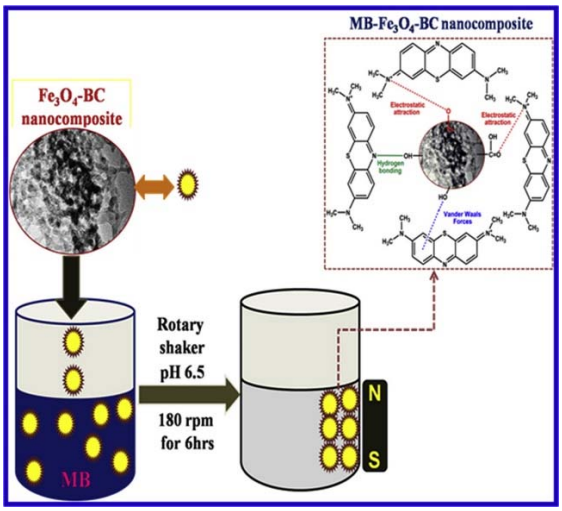

*Corresponding author: Tel: 012 420 3569 Email address: deon.brink@up.ac.za

Abstract

In this work hydrothermally prepared magnetic iron oxide coated biochar nanocomposite (Fe_3O_4-BC), from raw avocado peel (raw AVP) and ferric chloride hexahydrate, effectively adsorbed aqueous methylene blue (MB) dye. Successful Fe_3O_4-BC formation was confirmed by TEM, FT-IR, XRD and SEM. BET analyses measured a higher surface area (25.98 m^2/g vs 18.89 m^2/g) and smaller pore diameter (8.25 nm vs 13.01 nm) for Fe_3O_4-BC compared to raw AVP. The Tempkin and Langmuir isotherm models successfully modeled the Fe_3O_4-BCMB adsorption equilibrium data, indicating uniform adsorption binding energy and homogeneous single layer adsorption. The maximum Langmuir adsorption capacity q_{max} = 62.1 mg/g for MB compared well with previously reported values for low cost carbonaceous adsorbents. The temporal experimental data was best represented by the pseudo-second order and two-phase pseudo-first-order kinetic models suggesting that chemisorption dominated. Thermal studies indicated spontaneous endothermic adsorption ($\Delta G < 0$, $\Delta H > 0$). Fe_3O_4-BCshowed remarkable stability and reusability during four consecutive adsorption-desorption cycles. Compared to literature, Fe_3O_4-BC adsorption was markedly faster requiring between 1 and 3 orders of magnitude less time to reach equilibrium. Consequently, a significantly lower treatment time would be required industrially which, coupled with magnetic separation, reusability, and relatively high adsorption capacity of the adsorbent, highlights the unprecedented industrial potential of Fe_3O_4-BC nanocomposite as an adsorbent for the treatment of MB polluted waters.

KEYWORDS: Fe_3O_4-BC nanocomposite; Methylene blue; Adsorption; Isotherm models; Kinetic models; Thermodynamic studies;

1. Introduction

A major global challenge remains the detrimental contamination of water resources due to exponentially increasing populations as well as ballooning industrial activities. The economically important industries of dyes, pharmaceuticals, and pesticides discharge various types of pollutants to the hydrosphere, and by extension sourced of drinking water, which create severe human health and environmental problems [1]. Prominently, the dye industry is one of the largest producers of pollutants worldwide [2-5]. Contamination of water sources by toxic dyes, such as methylene blue, malachite green, and rhodamine B, not only causes significant environmental problems, it also poses severe risks to human health including carcinogenicity, kidney disfunction, and central nervous system disorders [6-15]. Among them methylene blue (MB) is a cationic dye, which is applied in various industries including dyeing, printing, chemical indicators, and biological applications [16, 17]. MB containing wastewaters pose serious risks to both microorganisms in the environment and human health due to large organic loads, reduced biodegradability, and high chromaticity [18]. Therefore, coordinated plans are required for the decrease of dye concentrations in effluents.

Recently, several methods have been proposed for the treatment of dye containing wastewater including physical, chemical, and biological approaches [19]. Specifically, different technologies have been investigated such as membrane filtration [20], flocculation [21], biodegradation [22], advanced oxidation [23], electrochemical method [24], photocatalytic degradation [25], and adsorption [26-28]. Adsorption is considered an efficient method for the treatment of dye wastewater because of low cost, ease of operation, large number of effective adsorbents, and better removal of toxic substances [29-32].

Over the past several years many researchers have tested different low-cost adsorbents such as sugarcane bagasse, wheat *Ficuscaricabast*, pinewood, biochar, switch grass, sludge, montmorillonite, flax fiber, zeolite, and clay for adsorption of dye from water [33-43]. Recently, biochar has been considered as an effective adsorbent derived from various agricultural wastes because of its large surface and variety of functional groups [44, 45]. However, biochar adsorbents are known to suffer from several disadvantages, such as poor adsorption capacity, agglomeration, and lower ability to be regenerated, for practical applications to be realized [46]. Consequently, biochar requires surface modification to improve surface properties and adsorption capacities which would result in cost-effective adsorbents for the removal of dye from aqueous solutions [47]. Different metal oxide modifications of various biochar nanocomposite have been studied, these include carboxymethyl cellulose stabilized ZnO/biochar nanocomposites [48], ZnO/cotton stalks biochar nanocomposite [49], Fe_3O_4-loaded biochar [50], biochar/Fe_xO_y composite [51], wheat shells [52], hazelnut shells [53], Al_2O_3 nanoparticle-coated biochars [54], ZrO_2 nanoparticles on biochar [55], Titanium dioxide-coated biochar composites [56], and biochar of jackfruit peel to fabricate biogenic magnetite-biochar nanocomposite [57]. Of these, iron oxide-based biochar nanocomposites were of great interest for the adsorption of dyes from aqueous solution due to large surface area, better magnetic properties, high active prevalence of surface sites which enhance the adsorption capacity of these adsorbents, and favourable regenerability [58, 59].

Perseaamericana is the botanical name of the avocado tree which is part of the Laurel family. It is widely cultivated in Mexico, Central America, and several tropical and subtropical areas around the world. The avocado fruit is familiarly used as a vegetarian food because of its high fat content, acting as an alternate to salads and sandwiches. This fruit is extensively produced

and consumed in South Africa resulting in the production of significant amounts of avocado peel waste [60].Even though peels are not in itself harmful to the environment, it has the potential to be reused and consequently to reduce the impact of the waste. Biochar based iron oxide nanocomposite from avocado waste has been studied for the adsorption of various organic and inorganic pollutants [61, 62]. However, the production of biochar-based iron oxide nanocomposite from avocado peels for the adsorption of MB dye is an as yet unexplored area of research with significant potential.

In the present work, the authors proposed the preparation of iron oxide (Fe_3O_4) coated biochar nanocomposite (Fe_3O_4-BC) from avocado fruit peel by a hydrothermal treatment method. Raw avocado peel (raw AVP) and Fe_3O_4-BC were characterized to assess the influence of surface activation on the raw AVP. The Fe_3O_4-BC nanocomposite was subsequently used as an adsorbent for the adsorption of MB to assess its adsorption performance. Further, the study assessed various adsorption process parameters including the effects of adsorbent dosage, pH, MB concentration, temperature, and contact time to determine the adsorption capacity and optimal conditions to maximize the percentage removal of MB dye. Finally, the temporal adsorption kinetics and isotherms were determined to elucidate the adsorption mechanism of MB on Fe_3O_4-BC nanocomposite.

2. Experimental sections

2.1. Materials

Avocado fruit were purchased from a local food market in South Africa. $FeCl_3.6H_2O$ and methylene blue were purchased from Sigma-Aldrich (St Louis, MO, USA). Hydrochloric acid (HCl) and sodium hydroxide (NaOH) and Ethanol were obtained from Merck chemical Company (Kenilworth, NJ, USA). Analytical grade of all the chemicals and reagents were used without purification. Deionized water was used in all experiments.

2.2. Preparation of Fe_3O_4-BC nanocomposite by hydrothermal method

The surface of raw avocado peels (raw AVP) was washed several times to remove impurities and residual fruit material. The peels were dried at 100 ºC for 12 h and ground to produce *circa* 6.0 g of a macro-sized brownish yellow powder. 4.0 g of raw AVP powder and 0.5 g of $FeCl_3.6H_2O$ were mixed with 80 mL distilled water in a 100 mL beaker and vigorously stirring for 1 hour. Then the solution was transferred into a 100 mL Teflon coated autoclave and heated to 180 ºC for 12 h. After cooling to room temperature, the prepared Fe_3O_4-BC nanocomposite precipitate was collected from the solution by centrifugation and washed with water and ethanol several times to remove residual impurities. Finally, a blackFe_3O_4-BC nanocomposite powder was obtained by drying at 100 ºC for 12 h. The schematic diagram of preparation of Fe_3O_4-BC nanocomposite is shown in Fig.1.

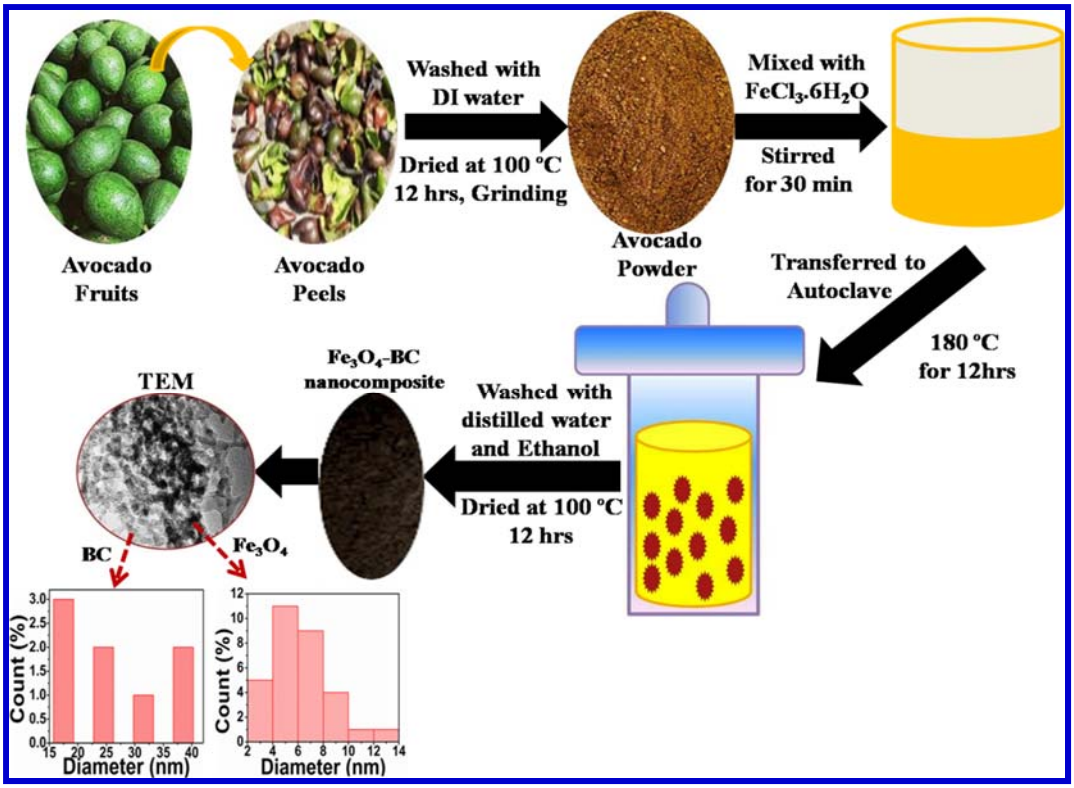

Figure 1. Schematic diagram of the preparation of Fe_3O_4-BC nanocomposite by hydrothermal method.

2.3. Characterization Techniques

The synthesized materials were characterized to confirm the successful formation of AVP and Fe_3O_4-BC nanocomposite. The surface functional groups were identified by Fourier Transform Infrared (FT-IR) (Perkin–Elmer PE1600 FTIR spectrophotometer, Perkin-Elmer, Waltham, MA) in the range of 4000–400 cm^{-1}. X-ray Diffractometer (XRD) determined the crystalline nature of all powders with a Panalytical X'Pert Pro X-Ray Diffractometer (Malvern Panalytical, Malvern, UK) and Philips PW1729 diffractometer (Phillips and Company, Amsterdam, Netherlands) with working systems of Cu Kα radiation (λ = 1.5406 Å) operating at 45 kV and 40 mA.The Raman spectra were used to identify the stretching vibration modes of the

nanoparticles (PerkinElmer Spectrum Two spectrometers, Perkin-Elmer, Waltham, MA) at a laser excitation line of 532 nm. The thermogravimetric (TGA) and Differential thermal analysis (DTA) properties of the nanomaterials were measured by using a TGA-DTA instrument (Netzsch, Selb, Germany) in the temperature interval of 50-900 °C. The Brunauer-Emmett-Teller (BET) method was utilized for determined the surface area and pore size under N_2 atmosphere adsorption-desorption process with a Micro-Metrics ASAP 2020 analyzer (Ottawa, Canada). The surface charge of materials was evaluated by zeta potential measurement with Malvern Zeta sizer NanoZS 90 (Malvern, UK). The morphology and elemental composition of the nanomaterials were investigated using a Scanning Electron Microscope (TESCAN, VEGA SEM, Brno, Czech Republic) at the electron acceleration voltage 20 kV with carbon coating for image quality. The size of nanomaterials was determined by using Transmission electron microscopy (TEM JEOL, JEM-2100F, Tokyo, Japan) with operating electron voltage of 90 kV. The pH measurements were performed with an OHAUS starter 2100 (Parsippany-Troy Hills, NJ, USA).

2.4. Batch adsorption

Evaluation of the adsorption activity of the MB dyeadsorbate on the Fe_3O_4-BC nanocomposite adsorbent was carried out by batch adsorption. 100 mL plastic bottles containing 50 mL of 15 mg/L initial concentration MB with various dosages of Fe_3O_4-BC nanocomposite adsorbent (10 to 80 mg), ata pH 6.5 was tested. Subsequently, Fe_3O_4-BC nanocomposite adsorbent mass (50 mg) was used for all equilibrium experiments. MB dye adsorption was also tested with different parameters: pH, adsorbate concentration,contact time and temperature. The plastic bottles were agitatedin a thermostatic shakerwater-bath (Labex Pty (Ltd), Johannesburg, South Africa) at 180 rpm for 6 h 0.45 μM PTFE membrane syringe filters were used toremove adsorbent from solution after termination of the adsorption equilibrium experiments. The equilibrium

concentrations of MB dye in the solution was determined at the maximum absorption wavelength of 664 nm using UV-visible spectrophotometer (Shimadzu UV-1208 model UV–visible spectrophotometer, Kyoto, Japan). 0.1 N HCl and 0.1 N NaOH solutions were used to adjust the pH during in the adsorption experiments. The percentage removal of MB,the temporal and equilibrium adsorbed amount of dye on Fe_3O_4-BC nanocomposite were calculated using equation (1) , (2) and (3). The adsorption experiments were carried out in triplicate and the average values determined.

$$\text{Removal efficiency (\%)} = \left(\frac{C_o - C_e}{C_o}\right) \times 100 \ldots\ldots\ldots\ldots\ldots\ldots (1)$$

$$q_t = \frac{C_0 - C_t}{M} \times V \ldots\ldots\ldots\ldots\ldots\ldots\ldots\ldots\ldots\ldots\ldots\ldots\ldots\ldots (2)$$

$$q_e = \frac{C_0 - C_e}{M} \times V \ldots\ldots\ldots\ldots\ldots\ldots\ldots\ldots\ldots\ldots\ldots\ldots\ldots\ldots (3)$$

Where q_t (mg/g) is the amount of dye on the adsorbent at time, q_e (mg/g) is the amount of dye on the adsorbent; C_0 and C_e are respectively initial concentration and equilibrium time of MB, V is the volume of solution and M is the mass of adsorbent.

2.5. Isotherm models

2.5.1. Langmuir isotherm model

The monolayer adsorption onto the surface of adsorbent with particular sites was determined by the Langmuir isotherm model. It can be written as equation (4) [63].

$$q_e = \frac{k_L q_{max} C_e}{1 + k_L C_e} \ldots\ldots\ldots\ldots\ldots\ldots\ldots\ldots\ldots\ldots\ldots\ldots\ldots\ldots (4)$$

where q_e is the MB concentration at equilibrium onto Fe_3O_4-BC nanocomposite adsorbent, q_{max} (mg g^{-1}) is the maximum adsorption capacity, C_e (mg/L) is the MB concentration at equilibrium and K_L (L/mg) is the Langmuir constant based the adsorption sites for MB.

The Langmuir isotherm can also be articulated with dimensionless separation factor (RL), which is described the favorable of adsorption method as follows equation (5) [64].

$$R_L = \frac{1}{1+C_0 \times K_L} \text{..... (5)}$$

Where K_L (L/mg) is the Langmuir constant and C_0 is the initial concentration of MB, R_L is the separated factor, which is mentioned the adsorption behavior of $R_L = 0$ (irreversible process), $R_L = 1$ (Linear), $R_L > 1$ (Unfavorable process) and $0 < R_L < 1$ (Favorable process) [65].

2.5.2. Freundlich isotherm model

The Freundlich isotherm model, which is an empirical model based on the multilayer adsorption on heterogeneous surfaces. The nonlinear term of the Freundlich equation for heterogeneous surface energy systems is given by equation (6) [66].

$$q_e = K_F C_e^{\frac{1}{n}} \text{.....(6)}$$

Where K_F is the adsorption capacity (mg/g) $(L/mg)^{1/n}$) and n is the Freundlich isotherm constant. The 1/n is the heterogeneous factor, which is related to the adsorption favorable of the adsorbent and adsorbate [67].

2.5.3. Tempkin isotherm model

The linear plot of Tempkin model is specified by using equation (7) [68]

$$q_e = \left(\frac{RT}{b_T}\right) \ln(K_T C_e) \text{.....(7)}$$

Where T is the temperature in Kelvin, R is the gas constant (8.314 J/mol K), b_T is the Tempkin constant(mg/L) and K_T is the Tempkin isotherm equilibrium constant in (L/g).

2.6. Reusability-adsorption/desorption studies

Adsorption/Desorption studies were tested by initial adsorption experiment using 50 mg of the Fe_3O_4-BC nanocomposite in 50 mL of MB solution (15 mg/L) into rotary water-bath thermal shaker with rotation speed 180 rpm at 25 °C for 2 hr. After that, desorption was conducted by rotator shaker the MB onto Fe_3O_4-BC nanocomposite with 20 mL (0.1 M) of HCl and 10 mL ethanol for 2h The regenerated Fe_3O_4-BC nanocomposite adsorbent was recovered by a strong magnet and then washed with distilled water and dried 70 ºC for 6 h before repeating the adsorption-desorption cycle at the same MB concentration. This desorption-desorption method was repeated for four cycles.

3. Results and discussion

3.1. FT-IR characterization

Figure 2A (a & b) shows the surface functional groups of raw AVP and Fe_3O_4-BC nanocomposite as identified by FT-IR spectroscopy. The raw AVP displayed peaks at 3424 cm^{-1}, 2926 cm^{-1}, 2865 cm^{-1}, 1736 cm^{-1}, 1635 cm^{-1}, 1448 cm^{-1} and 1046 cm^{-1}, corresponding to O-H, $=CH_2$, C-H, C=O, C=C, C-O-C and C−OH stretching vibration as shown in Fig.2A(a) [69-72]. For the Fe_3O_4-BC nanocomposite slightly shifted peak positions at 3385 cm^{-1}, 2916 cm^{-1}, 2854 cm^{-1}, 1705 cm^{-1}, 1619 cm^{-1}, 1457 cm^{-1}, and 1118 cm^{-1}were observed as compared to raw AVP. Additionally, peaks at 796 cm^{-1} and 612 cm^{-1}peaks were observed due to the formation stretching and vibration of Fe-O bond in the Fe_3O_4-BC nanocomposite, respectively, as shown in Fig.2A (b). The types of peaks were noted in previous reports [73-75].

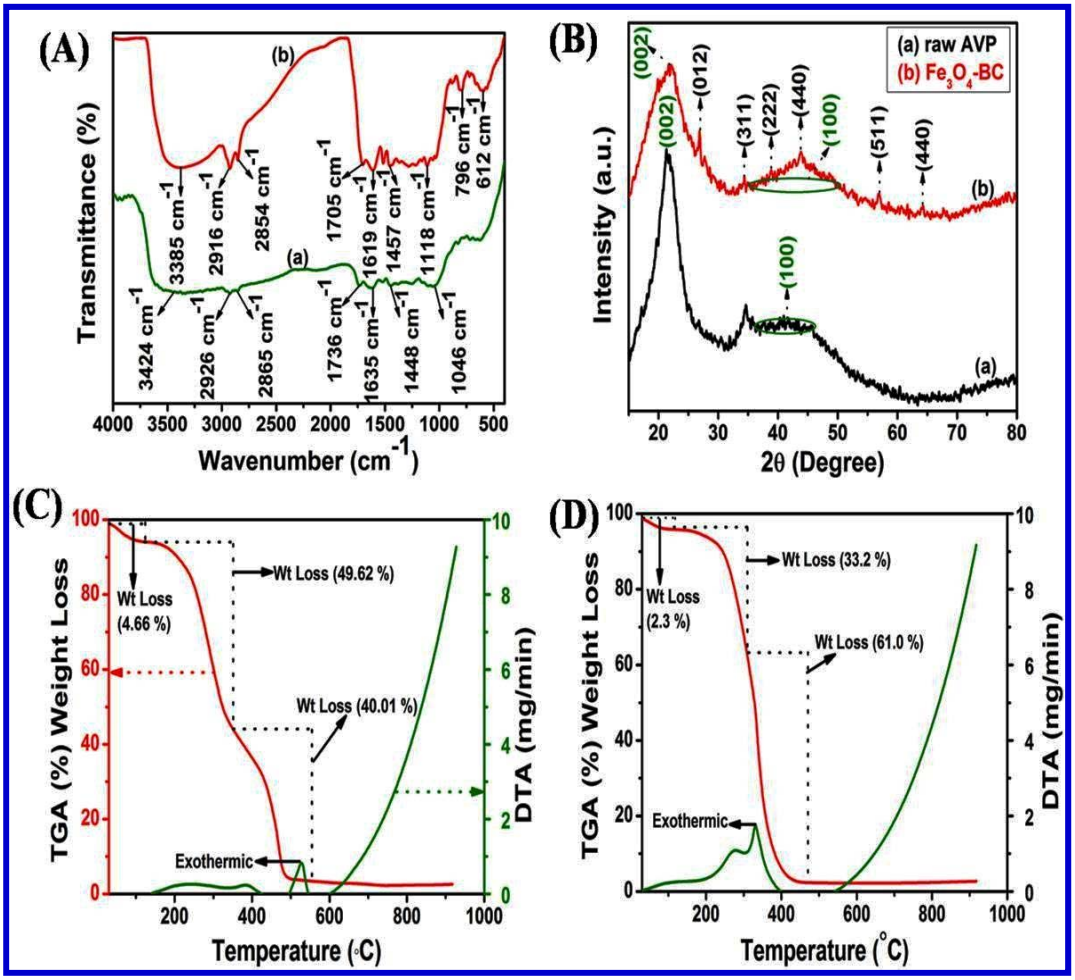

Figure 2 (A-D). (A) FT-IR spectra of raw AVP (a) and Fe_3O_4-BC nanocomposite (b), (B) X-ray diffraction of raw AVP and Fe_3O_4-BC nanocomposite and TGA/DTA spectra of (C) raw AVP and (D) Fe_3O_4-BC nanocomposite.

3.2. XRD characterization

The crystalline and amorphous nature of raw AVP and BC-Fe_3O_4 nanocomposite were conducted by XRD patterns as shown in Fig.2B (a&b). Sharp and broad diffraction peaks appeared at 2θ = 21.63º and 40.6º which are indicative of the amorphous nature of the carbon structure [76]. A small Intensity peak was observed at 34.5º and corresponded to the mixed inorganic components in the raw AVP as shown in Fig.2B (a) [77]. Figure 2B (b) show the different diffraction peaks at

2θ = 26.87°, 34.38°, 38.83°, 43.77° and 56.83° and 64.25° which are ascribed to (220), (311), (400), (422), (511) and (440) planes. This observation indicated the crystalline nature of Fe_3O_4 in the BC-Fe_3O_4 nanocomposite. Additionally, two small intensity broad peaks appeared at 2θ = 22.62° and 35.82° to 55.33°, which are assigned to the (002) and (100) planes of graphite carbon structures [78]. These diffraction peaks are characteristic of Fe_3O_4 (JCPDS no. 19–0629) [79, 80] and therefore indicating that $Fe_3O_4$was effectively coated on the surface of the BC. Further, the crystal size of the Fe_3O_4-BC nanocomposite (15.4 nm) was calculated using Scherrer equation (8).

$$D = k\lambda/\beta \cos\theta \quad (8)$$

Where D = average size of particles, K = Scherrer's constant (0.90), λ= radiation wavelength (1.5406 Å), β = full width at half maximum intensity (FWHM) given in radians and θ = Braggs diffraction angle.

3.3. TGA characterization

Thermal gravimetric analysis (TGA) quantified the thermal stability and thermal performance of AVP and Fe_3O_4-BC nanocomposite in N_2 atmosphere from 30 °C to 900 °C and heating rate of 5°C/min, and is shown in Fig.2(C&D), respectively. Figure 2(C) shows three distinct weight loss regions in the range of 30 to 120 °C, 120 to 350 °C and 350 to 550 °C, corresponding to the removal of moisture and organic volatile compounds, decomposition of major carbonization, and thermal decomposition of the organic backbone, respectively [81, 82]. Above 550 °C, indicated the dislocation of compounds and good stability. From the differential thermal analysis (DTA) spectrum it was evident that the decomposition was exothermic as shown in Fig.2 (C). The TGA spectrum of Fe_3O_4-BC nanocomposite also showed three weight loss regions:30 to 115 °C, 115 to 310 °C and 310 to 470 °C due to the elimination of water molecules and organic

matter, decomposition of main carbonization, and decomposition of the structure of Fe-O in Fe_3O_4-BC nanocomposite, respectively, as shown in Fig.2(D). Above 470 $^{\circ}$C, the Fe_3O_4-BCdemonstratedimprovedthermal stability (negligible weight loss) [83].The DTA spectrum indicated an exothermic reaction as shown in Fig.2D.

3.4. BET characterization

The specific surface area, and pore size of AVP and Fe_3O_4-BC nanocomposite were characterized by N_2 adsorption-desorption isotherms with BET analysis as shown in Supporting Information Fig.S1A (a&b). The BJH plots which were used to evaluate the surface area of AVP (18.89 m^2/g) and Fe_3O_4-BC nanocomposite (25.98m^2/g), these plots shows that the N_2adsorption-desorption exhibited type IV isotherm behaviour with H3 hysteresis loops indicative of mesoporous materials as shown in Supporting Information Fig.S1A(a&b) [84, 85]. Pore size distribution of AVP (13.01 nm) and Fe_3O_4-BC nanocomposite (8.25 nm) as measured from the BJH plot as shown in Supporting Information Fig.S1B (a&b). From the Supporting Information Figure S1B (a&b), Fe_3O_4-BC nanocomposite was observed to have a much high surface area and smaller pore size than AVP, indicating that the Fe_3O_4 coated on BC showed good dispersity in the water medium [86].

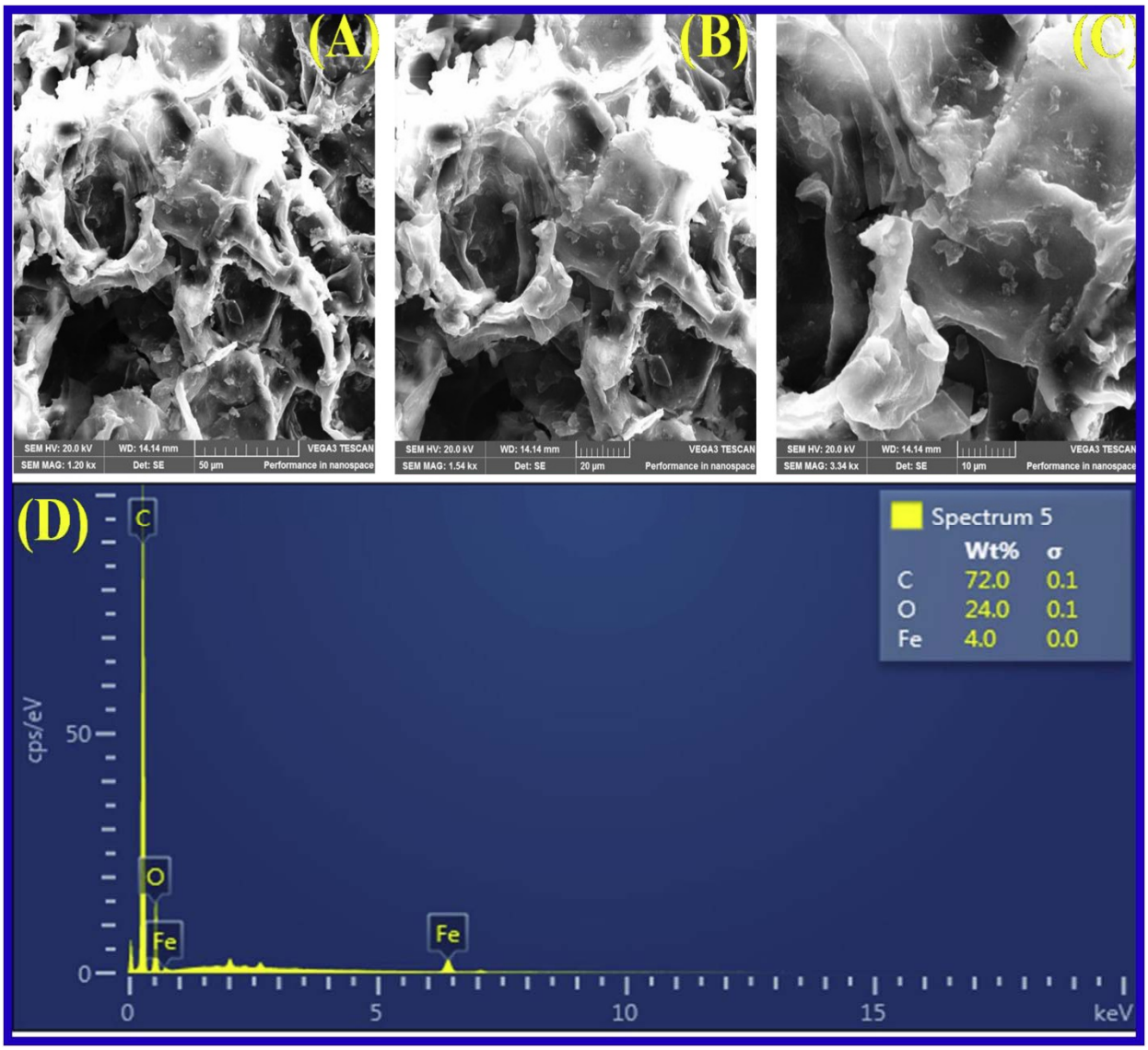

Figure 3 (A-D). SEM images of Fe_3O_4-BC nanocomposite of (A) 50 µm, (B) 20 µm and (C) 10 µm and (D) EDAX image of Fe_3O_4-BC nanocomposite.

3.5. SEM characterization

The morphology of Fe_3O_4-BC nanocomposite was determined by scanning electron spectroscopy as shown in Fig.3 (A-C). The surface image of Fe_3O_4-BC nanocomposite was observed at various magnifications 20 µm, 10 µm and 5 µm. Figure 3A (a) shows the unequal white particles with porous nature of sheet image was recorded at low magnification 50 µm as

shown in Fig.3A. The white particles bounded on porous sheet was clearly observed at high magnifications at 20 μm and 10 μm magnifications as shown in Fig.3(B&C). The elemental composition of Fe_3O_4-BC nanocomposite was done by EDAX analysis (Figure 3D) indicating the presence of C, O and Fe and therefore confirming that Fe_3O_4 successfully coated on BC.

3.6. TEM characterization

The shape and size of the Fe_3O_4-BC nanocomposite as investigated by TEM as shown in Supporting Information Figure S2 (A-C). The dark particles coated on porous thin sheets of BC were captured at various areas with the same magnification of (as indicated by 100 nm bar) Supporting Information Figure S2 (A&B). The dark particles of Fe_3O_4 and porous of BC were clearly explored at high magnification (note 50 nm bar) indicated by yellow arrow as shown in Supporting Information Figure S2 (C).

3.7. Removal of MB by batch adsorption

3.7.1. Effect of dosage

The optimal dosage was investigated for the removal of MB (15mg/L, 50 mL) with different dosage (10, 20, 30, 40, 50, 60,70 and 80mg) of Fe_3O_4-BC nanocomposite were used at180 rpm for 6 hours, at a near-neutral pH 6.5. Figure 4A (a) shows the percentage of removal of MB (99.06 to 99.52 %) increased with increased dosage of 10 to 50mg resulting from the higher availability of adsorbent sites with Fe_3O_4-BC nanocomposite adsorbent. Even though, the percentage removal of MB was slightly decreased with further increased dosage of 60–80 mg due to agglomeration of adsorbent, which reduces the available surface of Fe_3O_4-BC nanocomposite adsorbent [87]. The amount of MB adsorbed on Fe_3O_4-BC nanocomposite adsorbent was also displayed with different dosages as shown in Fig.4A (b). The spectra and digital images of before

and after adsorption of MB with optimum dosage of 50 mg were displayed as shown in Fig.4B (inset). This was similarly reported for removal of MB with other adsorbents [88, 89].

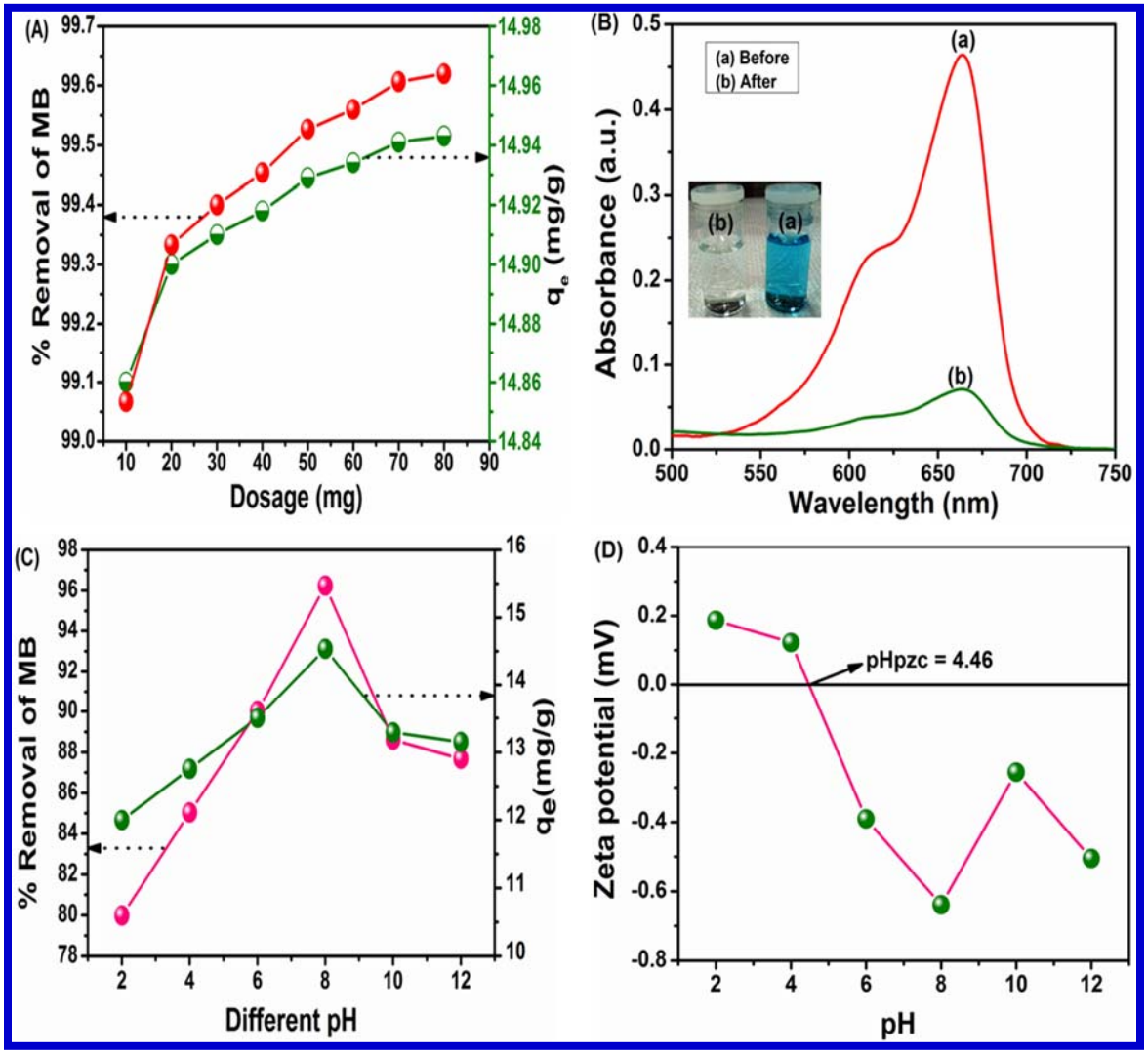

Figure 4 (A-D). (A) Effect of dosage on MB adsorption by Fe_3O_4-BC nanocomposite, (B) UV-visible spectra of before and after adsorption MB with 50 mg dosage of Fe_3O_4-BC nanocomposite, (C) Effect of pH on MB adsorption Fe_3O_4-BC nanocomposite and (D) Zeta potential of Fe_3O_4-BC nanocomposite with various pH 2, 4, 6, 8, 10 and 12.

3.7.2. Effect of pH and Zeta Potential

The pH is an important factor in adsorption of MB onto Fe_3O_4-BC nanocomposite adsorbent, which aids in understanding the mechanism of adsorption by providing information on the surface charge of the adsorbent and MB in solution. Figure 4(C) showed the adsorption of MB onto Fe_3O_4-BC nanocomposite as conducted with different pH values of 2, 4, 6, 8, 10 and 12. At the pH2 to pH 8 adsorption of MB was slightly increased because of repulsion between the positive charge of adsorbent and positive charge of MB in the acidic solution [90]. The data showed the maximum adsorption removal efficiency at pH 8 due to strong interaction between the negative charge of Fe_3O_4-BC and positive charge of MB in the basic medium [91]. Above pH8 the adsorption of MB was slightly decreased due to increased negative charge onto MB and Fe_3O_4-BC nanocomposite [92]. Figure 4(D) shows the zeta potential of Fe_3O_4-BC nanocomposite decreased from +0.187 mV to –0.505 mV with increasing the pH 2 to pH 12. The slight increase in zeta potential at pH 10 is likely a result of the deposition of charged particles on the nanocomposite surface. Further the point of zero charge (pHpZc) was calculated at 4.46 and Fe_3O_4-BC nanocomposite adsorbent surface is neutral, the pH reaches equilibrium as pHpzc [93]. This means that the Fe_3O_4-BC nanocomposite has a positive charge below pH of 4.46. At pH lower than pHpzc the material opposed the removal of MB and higher than pHpzc the Fe_3O_4-BC nanocomposite becomes negative charge to enhance the removal of MB due to electrostatic interaction. The adsorption of MB decreased when the pH solution is reached at a higher rate due to repulsion between the negative charge surface of adsorbent and negative charge of adsorbate [94].

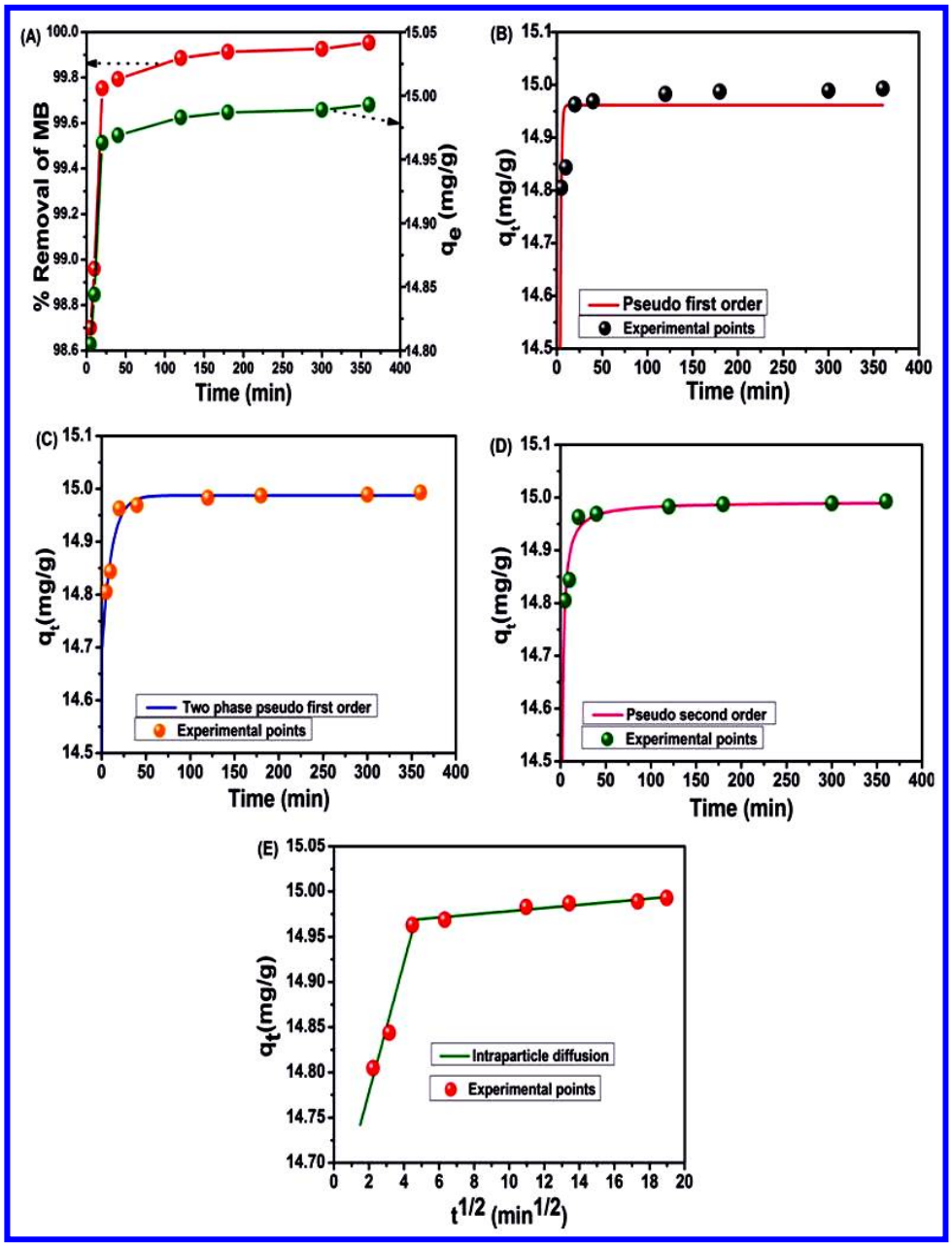

Figure 5(A-D). (A) Effect of contact time on MB adsorption with Fe_3O_4-BC nanocomposite with nonlinear plot, (B-D) Nonlinear plot of pseudo first order kinetic, two-phase pseudo-first order and second order kinetic plots for MB adsorption with Fe_3O_4-BC nanocomposite and (E) Intraparticle diffusion model for adsorption of MB onto the Fe_3O_4-BC nanocomposite.

3.7.3. Effect of contact time

To determine the effect of contact time on the adsorption of MB (15 mg/L in 50 mL) onto Fe_3O_4-BC nanocomposite (50 mg), samples were taken at different contact times5, 10, 20, 40, 120, 180, 300 and 360 min at a temperature of 25 ºC. Figure 5 (A) shows that nearly complete removal of MB was observed as early as 5 minutes (98.7 %) for Fe_3O_4-BC nanocomposite and then effectively complete equilibrium was obtained after 120min (99.9 %). The adsorbent initially has more available sites to enhance removal of MB which then decrease with increased removal of MB due to less vacant sites on the Fe_3O_4-BC nanocomposite [95].

3.7.4. Adsorption kinetics

From Figure 5 (A), the determination of the adsorption kinetic mechanism of MB removal with Fe_3O_4-BC nanocomposite was conducted by using experimental fitting of the kinetic data with pseudo-first-order, pseudo second-order and two-phase pseudo-first order as well as intra-particle diffusion models as shown in Fig.5 (B-E). The nonlinear term of the pseudo first order rate model is expressed by equation (9) [96].

$$q_t = q_e(1 - e^{-k_1 t}) \text{.....(9)}$$

Where, q_e and q_t are the amount of MB adsorbed on Fe_3O_4-BC nanocomposite at equilibrium and time t (mg/g) and k_1 is the first order rate constant (min^{-1}).

The nonlinear solution of the pseudo second order model can be expressed by equation (10) [97]

$$q_t = \frac{(k_2 q_e^2)t}{1+k_1 q_e t} \text{.....(10)}$$

where q_e is the amount of MB adsorbed per unit mass of Fe_3O_4-BC nanocomposite at equilibrium (mg/g), q_t is the amount of MB adsorbed at contact time t (mg/g) and $k_2$is the pseudo second order rate constant (g/mg min)[98].

The nonlinear solution of the two-phase pseudo-first order model is shown in Eq. (11) [99]

$$q_t = q_e\phi_{fast}\left[1 - exp\left(-k_{1,fast}t\right)\right] + q_e\left(1 - \phi_{fast}\right)\left[1 - exp\left(-k_{1,slow}t\right)\right] \ldots\ldots (11)$$

where q_t is the amount of MB adsorbed at contact time t (mg/g), q_e is the amount of MB adsorbed per unit mass of Fe_3O_4-BC nanocomposite at equilibrium (mg/g), ϕ_{fast} is the fraction of the adsorption capacity attributed to fast adsorption, $k_{1,fast}$ is the fast adsorption reaction pseudo first order reaction rate constant and $k_{1,\ slow}$ is the slow adsorption reaction pseudo first order reaction rate constant.

The pseudo first order, two-phase pseudo-first order and second order kinetic models were described as non-linear plots and their results for the removal of MB onto Fe_3O_4-BC nanocomposite as shown in Table 1. The kinetic models were estimated with correlation coefficient (R^2) value in which pseudo second order (R^2 = 1) and two-phase pseudo-first-order (R^2 =1) are higher than the pseudo first order (R^2 = 0.9999). From the kinetic models, the pseudo second order and two-phase pseudo-first-order provided a better description of the removal and indicates that the adsorption of MB onto Fe_3O_4-BC nanocomposite rate limiting step is likely chemisorption dominated by valence forces during the exchange and sharing of electrons [100, 101]. An important model providing information on adsorption process in the removal of MB with Fe_3O_4-BC nanocompositeis the intra-particles diffusion model. This model is considered to provide insight into the relative external adsorption uptake from the boundary layer at the adsorbent surface or diffusion within the adsorbent [102]. If the Weber and Morris plot display a straight line with passing during zero, the adsorption process is controlled by intraparticle diffusion model and if the plot does not pass through zero it is not a diffusion rate-controlled process [103].

Table 1 Kinetic parameters of the nonlinear forms of pseudo-first-order model, two-phase pseudo-first-order, pseudo-second-order model, and intra particle diffusion model for adsorption of MB onto Fe_3O_4-BC nanocomposite at 25 ºC.

Kinetic Models	**Parameters**	**Fe_3O_4-BC nanocomposite**
Pseudo-first-order	q_e (mg/g)	14.96
	k_1 (1/min)	0.9086
	R^2	0.9999
Two-phase pseudo-first-order	q_e (mg/g)	14.99
	k_{1fast} (1/min)	125.1
	k_{1slow} (1/min)	0.09244
	R^2	1.000
Pseudo-second-order	q_e (mg/g)	14.99
	k_2 (g/mg.min)	0.9659
	R^2	1.000
Intra-particle diffusion	$K_{int,1}$ (mg/g.min$^{1/2}$)	0.07201
	$C_{i,1}$ (mg/g)	14.64
	$K_{int,2}$ (mg/g.min$^{1/2}$)	0.001741
	$C_{i,2}$ (mg/g)	14.96
	R^2	1.000

Figure 5 (E) shows the linear plot q_t against $t^{1/2}$ was obtained by the intra-particle diffuse model, also known as the Weber-Morris model [104]. The linear plot indicated the MB which was adsorbed from the boundary layer at the surface of the Fe_3O_4-BC nanocomposite. The system was not limited by a rate controlling adsorption process of MB onto Fe_3O_4-BC nanocomposite because of line did not pass through zero [105]. The kinetic data were applied to equation (12) as given below.

$$q_t = k_{int} t^{\frac{1}{2}} + C \quad \text{..... (12)}$$

Where, k_{int} is the intraparticle diffusion rate constant (mg/g $min^{1/2}$), C_i is the intercept based on the thickness of outer layer and confirms that the adsorption of MB onto Fe_3O_4-BC nanocomposite was a multi-step method connecting adsorption onto outer layer surface and diffusion into the inside pore [106]. The results were calculated from Figure 5 (E) and reported in Table 1.

3.7.5. Effect of concentration MB and adsorption isotherm

Different initial concentrations of MB (5-30 mg/L) were evaluated for adsorption behavior with a constant adsorbent dosage of 50 mg in 50mL, temperature of 25 °C and a pH 6.5 and the results are shown in Fig.6(A). The percentage efficiency (99.77-99.83 %) was increased with increasing concentration range of MB (5 -15 mg/L) and additionally percentage removal of MB was decreased with increased concentration MB (20-30 mg/L) and digital image of after adsorption is shown in Fig.6(A) (insert). The equilibrium adsorption capacity was increased as the initial concentration of MB, while the removal of MB decreased as the initial concentration increases as shown in Fig.6(A). This means that the driving force for mass transfer of MB towards adsorbed on the active site of Fe_3O_4-BC nanocomposite surface [107].

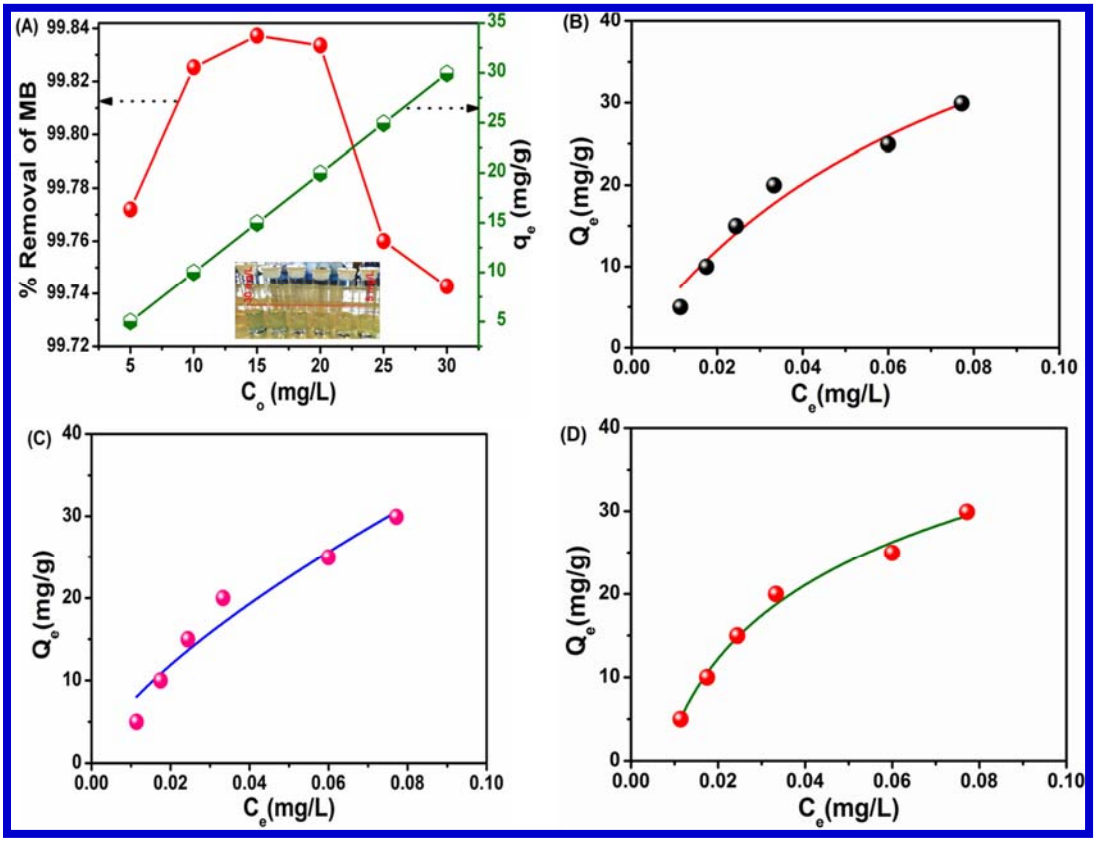

Figure 6 (A-D). (A) Effect of initial concentration of MB on adsorption with Fe_3O_4-BC nanocomposite with nonlinear plot, (B) Nonlinear Langmuir isotherm model, (C) Nonlinear Freundlich isotherm Model and (D) Nonlinear Tempkin isotherm model.

The adsorption results were investigated by using different isotherm models *viz.* Langmuir, Freundlich, and Tempkin isotherms to find the maximum adsorption capacity (q_m) of the Fe_3O_4-BC nanocomposite at equilibrium for the different initial concentrations of adsorbate of MB by using equations 4, 6 and 7. The Tempkin model presented the best fit with the correlation coefficient R^2=0.9914 and the Langmuir model (R^2 = 0.9685), the fits are shown in Fig.6(B-D). These results indicate that the adsorption process was likely characterized by uniform binding energy, favoring single layer adsorption on a homogeneous surface [108-111**].** The adsorption

equilibrium parameters were shown in Table 2. The Fe_3O_4-BC nanocomposite demonstrated comparable adsorption capacity for removal of MB from wastewater.

Table 2 Nonlinear forms of isotherm models parameters for adsorption MB onto Fe_3O_4-BC nanocomposite at 25 °C.

Isotherm models	**Parameters**	**Fe_3O_4-BC nanocomposite**
Langmuir model		
R^2	-	0.9685
q_m	mg g^{-1}	62.1
K_L	L mg^{-1}	12.0
R_L	-	0.0164 – 0.00277
Freundlich model		
R^2	-	0.9507
1/n	-	0.700
K_F	$(mg/g)(L/mg)^{1/n}$	183.5
Temkin model		
R^2	-	0.9914
K_T	L/mg	130.6
b_T	J/mol	194.3

3.7.6. Thermodynamics

The effect of the temperatures298, 308 and 318 K on the adsorption of MB (15 mg/L) onto Fe_3O_4-BC nanocomposite (50 mg/50 mL) was determined and consequently the free energy (ΔG),

enthalpy (ΔH), and entropy (ΔS) of adsorption were determined. These values were calculated by using the following equation (13-16) [112].

$$\Delta G = -RT\ln K_L \quad \text{.....(13)}$$

$$K_L = \frac{q_e}{C_e} \quad \text{.....(14)}$$

$$\Delta G = \Delta H - T\Delta S \quad \text{.....(15)}$$

$$\ln K_L = \frac{\Delta S}{R} - \frac{\Delta H}{RT} \quad \text{.....(16)}$$

q_e (mg/g) is the adsorption capacity of MB at equilibrium with Fe_3O_4-BC nanocomposite, C_e (mg/L) is the equilibrium MB concentration, R is the gas constant (8.314 J/mol K), ΔG (kJ/mol) is the Gibbs free energy of sorption which was calculated using equation (8). The enthalpy ΔH (kJ/mol) and entropy ΔS (kJ/mol/K) of adsorption were obtained from the slope and intercepts of the plot of $\ln K_L$ versus 1/T. The adsorption capacity increased with increasing temperature from 298 to 318 K as shown in Supporting Information Fig.S3 (A). The experimental results confirmed that the adsorption was and endothermic process due to the positive ΔH (34.9061 kJ/mol) value as shown in Supporting Information Fig.S3 (B) [113]. Fe_3O_4-BC nanocomposite displayed the highest adsorption capacity at 45 °C due to the endothermic nature of the adsorption in which the adsorption equilibrium shifted towards the adsorbed state with increased temperature [114]. Further the positive value of entropy change, ΔS (0.1698kJ/mol K) reflects the affinity of MB between Fe_3O_4-BC nanocomposite is shown in Table 3. The calculated negative values of ΔG (-15.4849, -17.8814, -18.8509 kJ/mol) indicates spontaneous nature of the adsorption process [115].

Table 3 Thermodynamic parameters for the removal of MB by using Fe_3O_4-BC nanocomposite.

Temperature (K)	ΔG (KJ/mol)	ΔH KJ/mol)	ΔS (KJ/mol)
298	-15.4849	34.9061	0.1698
308	-17.8814		
318	-18.8509		

3.7.7. Reusability-adsorption/desorption studies

Investigating the recycling of an adsorbent is a critically important part of the adsorption study as it provides a measure of the reusability which would demonstrate an improved economic advantage of the adsorbent and concomitantly minimized sludge yield. The removal of MB with Fe_3O_4-BC nanocomposite was conducted at various pH values (see section 3.7.2). Markedly lower removal of MB was observed in acidic medium with Fe_3O_4-BC nanocomposite as shown in Supporting Information Fig.S4 (C). For the reusability study, initially 15 mg/L in 50 mL of MB dye solution was adsorbed onto 50 mg of Fe_3O_4-BC nanocomposite for 2hrs at 180 rpm and25 °C. The adsorbent was magnetically separated and the supernatant was collected to determine the residual concentration of MB in the solution by UV-visible spectroscopy. Subsequently the MB-Fe_3O_4-BC nanocomposite was washed with distilled water and dried at70 °C for 6h. After drying the 20 mL of 0.1 M HCl and 10 mL ethanol were added to theMB-Fe_3O_4-BCand stirred for 1h and then filtered magnetically to evaluate the concentration of desorbed MB in the solution the same way as for the absorption experiment. Additionally, separated Fe_3O_4-BC nanocomposite was washed with distilled water and then dried in hot air oven at 70 °C to get regenerated Fe_3O_4-BC nanocomposite for reuse. This cycling was repeated four times.

The percentage of adsorption of MB versus cycle number was plotted as shown in Supporting Information Fig.S4 (A). The Fe_3O_4-BC nanocomposite demonstrated good reusability from the first to third cycles with adsorption efficiency (89.78 %, 87.82 % and 76.73 %) while the adsorption efficiency (46.08%) decreased markedly with the fourth cycle. The UV-visible spectra for the reusability-adsorption for four cycles, with a clarifying image, are shown in Supporting Information Fig.S4 (B) (inset). Supporting Information Figure S4 (C) shows the plot of percentage desorption efficiency versus number cycles and it was obtained by using equation (17).

% desorption efficiency = Mass of MB desorbed/Mass of MB adsorbed ×100…….. (17)

The desorption efficiency of MB fromFe_3O_4-BC nanocomposite was evaluated as first cycle = 36.85 % and second cycle = 21.52 %, third cycle = 17.97% and fourth cycle = 7.86 %. The MB recovery was also confirmed with UV-visible spectra with four desorption cycles as shown in Supporting Information Fig.S4 (D).

3.7.8. Comparison of kinetic and isotherm parameters to previous studies

The system parameters measured in this study was compared to the corresponding parameters from literature studies utilizing low cost carbonaceous adsorbents and shown in Table 4. The parameters under consideration were the Pseudo first order reaction rate constant (k_1), the Pseudo second order reaction rate constant (k_2), the equilibrium adsorption capacity from the pseudo second order model (q_e), and the maximum adsorption capacity obtained from the Langmuir adsorption isotherm (q_m). In addition, to facilitate comparison between the kinetic parameters, the times to reach 99% of the equilibrium adsorption capacity from the Pseudo first order model – using equation (9) – (PFO t_{99}) and the pseudo second order model – using equation (10) – (PSO t_{99}) were calculated and shown in Table 4 for all the systems compared. It should be

Table 4 Comparison of different system parameters dictating MB adsorption onto Fe_3O_4-BC nanocomposite with different adsorbents.

Adsorbent	k_1 (1/min)	PFO t_{99} (min)	k_2 (g/mg.min)	q_e (mg/g)	PSO t_{99} (min)	q_m (mg/g)	Reference
Enteromorpha prolifera AC	0.05	92.1	0.000077	263.2	4872.28	270.27	27
Ficus carica bast AC	0.02	224.64	0.00019	55.56	9378.2	47.62	38
Sewage sludge biochar	0.04 ± 0.03	498.26 ± 724.49	0.05 ± 0.08	15.81 ± 7.04	1124.73 ± 1177.47	24.1	39
wheat straw	0.03	159.9	0.0008	54.11	2287.01	60.66 ± 1.61	45
Sorghum straw Biochar	0.02	244.11 ± 29.07	0.00035±0.00021	95.36 ± 67.17	3801.06 ± 475.01	111.66	50
Banana peel biochar	0.06 ± 0.03	95.63 ± 56.3	0.0014	64.61 ± 30.67	1696.96 ± 945.54	562	51
Wheat Shells	0.04	131.58	0.004	17.92	1381.14	16.56	52
Hazelnut shells	0.12 ± 0.09	73.94 ± 61.83	0.04 ± 0.08	36.73 ± 22.45	1098.13 ± 1198.97	59.1	53
Walnut	0.12 ± 0.09	58.28 ± 39.94	0.13 ± 0.22	36.73 ± 28.33	623.81 ± 687.56	59.17	53
Cherry	0.11 ± 0.12	82.31 ± 55.58	0.05 ± 0.09	28.97 ± 20.76	1313.53 ± 1071.5	39.84	53
Oak	0.12 ± 0.09	54.19 ± 29.97	0.13 ± 0.22	19.4 ± 12.9	421.16 ± 349.06	29.94	53
Pitch-pine	0.11 ± 0.1	66.09 ± 39.76	0.13 ± 0.22	18.87 ± 12.25	630.3 ± 502.84	27.78	53
Fe_3O_4-BC nanocomposite	**0.91**	**5.07**	**0.97**	**14.99**	**6.84**	**62.1**	**This work**

noted that the PFO t_{99} is independent of q_e and therefore provides a better comparison between systems operated at different adsorbate concentrations. The table clearly shows that that the current adsorbent has reaction kinetics between 1 and 2 orders of magnitude faster than other adsorbents based on the PFO t_{99} values and up to three orders of magnitude faster to equilibrium based on the PSO t_{99} values. In and industrial application utilizing a continuous treatment system this would be invaluable as the fast kinetics mean a much lower residence time is required. This provides the potential for a much greater volume turnover and faster treatment rate which, coupled with the potential for continuous magnetic removal of the adsorbent, favorable adsorption capacity, and good reusability, provides previously unprecedented scaling potential.

3.7.9. Adsorption Mechanism

The adsorption mechanism of MB with Fe_3O_4-BC nanocomposite process is explained as shown in Supporting Information Fig.S5. Fe_3O_4-BC nanocomposite is a negatively charged adsorbent due to the presence of OH, COOH and Fe-O groups on the surface. MB is appositively charged dye because of quaternary ammonium, sulfur and nitrogen. The functional groups from both adsorbent (Fe_3O_4-BC) and adsorbate (MB) effectively interacted which resulted in hydrogen bonding, electrostatic interaction, and Vander Waals forces [116]. Additionally, The FT-IR spectra and SEM were characterized before and after adsorption of MB onto Fe_3O_4-BC nanocomposite adsorbent as shown in Supporting Information Fig.S6 (A&B). FT-IR peaks were not altered in peak position however a few peaks were shifted - specifically the wave numbers from 3385 to 3409 cm^{-1}, 1118 to 1108 cm^{-1}, and 612 to 596 cm^{-1} before and after adsorption of MB as shown in Supporting Information Fig.S6 (A). This clearly indicate that the OH, C-OH and Fe-O in the Fe_3O_4-BC nanocomposite played a crucial role in the uptake of MB from the wastewater solution

and a less intense peak was indicated with dotted line, which is confirmed that MB adsorbed onto Fe_3O_4-BC nanocomposite. SEM images also shows that the morphology of the adsorbent did not change markedly after adsorption of MB due to good stability and better reusability as shown in Supporting Information Fig.S6 (B).

4. Conclusions

In this study Fe_3O_4-BC nanocomposite was prepared by a hydrothermal method from raw avocado peel (AVP) and $FeCl_3.6H_2O$ as precursors. The Fe_3O_4-BC nanocomposite was subsequently evaluated for the adsorption of MB dye from wastewater. Fe_3O_4-BC nanocomposite was shown to have a higher surface area and smaller pore diameter than raw AVP. The adsorption study showed good maximum adsorption capacity for the removal of MB from aqueous solution (q_{max} = 62.1 mg/g). Good agreement with the experimental data of MB onto Fe_3O_4-BC nanocomposite was obtained with the Tempkin and Langmuir isotherm models and pseudo-second-order and two-phase pseudo-first-order kinetic models. Reusability of the Fe_3O_4-BC nanocomposite revealed good adsorption-desorption capacities and good stability after four cycles. Comparison of the system parameters with literature showed that the current system is between 1 and 3 orders of magnitude faster to equilibrium than previously reported which, coupled with the magnetic separation, reusability, and relatively high adsorption capacity demonstrates that theFe_3O_4-BC nanocomposite obtained from raw AVP has good potential to act as an economically viable adsorbent for the removal of MB from wastewater.

Author contribution statement

Eswaran Prabakaran: planned the project, data interpretation, wrote the first draft, **Kriveshini Pillay**: Visualization and study, **Hendrik Brink:** Supervision, writing, review, and editing.

Notes

The authors declare no competing financial interest.

ACKNOWLEDGMENTS

We thank the University of Pretoria (Postdoctoral fellowship) for the financial support and the University of Johannesburg, Johannesburg, South Africa for providing research facilities for this work.

References

[1] J.Martín, M. del Mar Orta, S. Medina-Carrasco, J.L. Santos, I. Aparicio, E. Alonso, Removal of priority and emerging pollutants from aqueous media by adsorption onto synthetic organo-funtionalized high-charge swelling micas. Environ. Res. 164 (2018) 488-494. https://doi.org/10.1016/j.envres.2018.03.037.

[2] P. Xu, M. Zheng, N. Chen, Z. Wu, N. Xu, J. Tang, Z. Teng, Uniform magnetic chitosan microspheres with radially oriented channels by electrostatic droplets method for efficient removal of Acid Blue. J Taiwan Inst Chem Eng. 104 (2019) 210-218.https://doi.org/10.1016/j.jtice.2019.09.016.

[3] S.N. Jain, S.R. Tamboli, D.S. Sutar, S.R. Jadhav, J.V. Marathe, A.A. Shaikh, A.A. Prajapati, Batch and continuous studies for adsorption of anionic dye onto waste tea residue: kinetic, equilibrium, breakthrough and reusability studies. J. Clean. Prod. 252 (2020) 119778.https://doi.org/10.1016/j.jclepro.2019.119778.

[4] P. Mehdizadeh, Y. Orooji, O. Amiri, M. Salavati-Niasari, H. Moayedi. Green synthesis using cherry and orange juice and characterization of $TbFeO_3$ ceramic nanostructures and their application as photocatalysts under UV light for removal of organic dyes in water. J. Clean. Prod. 252 (2020) 119765.https://doi.org/10.1016/j.jclepro.2019.119765.

[5] Y.W. Kim, J.H. Kim, D.H. Moon, H.J. Shin, Adsorption and precipitation of anionic dye Reactive Red 120 from aqueous solution by aminopropyl functionalized magnesium phyllosilicate. Korean J Chem Eng. 36 (2019) 101-108.doi: 10.1007/s11814-018-0168-8.

[6] A.I. Abd-Elhamid, E.A. Kamoun, A.A. El-Shanshory, H.M. Soliman, H.F. Aly, Evaluation of graphene oxide-activated carbon as effective composite adsorbent toward the removal of cationic dyes: Composite preparation, characterization and adsorption parameters. J. Mol. Liq. 279 (2019) 530-539.https://doi.org/10.1016/j.molliq.2019.01.162.

[7] A.M. Aljeboree, A.N. Alshirifi, A.F. Alkaim, Kinetics and equilibrium study for the adsorption of textile dyes on coconut shell activated carbon. Arab. J. Chem. 2017; 10:S3381-S3393.https://doi.org/10.1016/j.arabjc.2014.01.020.

[8] S. Tian, S. Xu, J. Liu, C. He, Y. Xiong, P. Feng, Highly efficient removal of both cationic and anionic dyes from wastewater with a water-stable and eco-friendly Fe-MOF via host-guest encapsulation. J. Clean. Prod. 239 (2019) 117767.

[9] T. He, J.-Q. Hua, R.-P. Chen, L. Yu, Adsorption characteristics of methylene blue by a dye-degrading and extracellular polymeric substance-producing strain. J. Environ. Manage. 288 (2021) 112446.https://doi.org/10.1016/j.jenvman.2021.112446.

[10] X. Jv, X. Zhao, H. Ge, J. Sun, H. Li, Q. Wang, H. Lu, Fabrication of a magnetic poly (aspartic acid)-poly (acrylic acid) hydrogel: application for the adsorptive removal of organic dyes from aqueous solution. J. Chem. Eng. Data. 64 (2019) 1228-1236. https://doi.org/10.1021/acs.jced.8b01117.

[11] W. Wang, Y. Zhao, H. Bai, T. Zhang, V. Ibarra-Galvan, S. Song, Methylene blue removal from water using the hydrogel beads of poly (vinyl alcohol)-sodium alginate-chitosan-montmorillonite. Carbohydr. Polym. 198 (2018) 518-528.https://doi.org/10.1016/j.carbpol.2018.06.124.

[12] E. Altıntıg, H. Altundag, M. Tuzen, A. Sarı , Effective removal of methylene blue from aqueous solutions using magnetic loaded activated carbon as novel adsorbent,Chem. Eng. Res. Des. 122 (2017) 151-163.https://doi.org/10.1016/j.cherd.2017.03.035.

[13] E Altıntıg, M Yenigun, A Sarı, H Altundag,M.uzen, T.A.Saleh, Facile synthesis of zinc oxide nanoparticles loaded activated carbon as an eco-friendly adsorbent for ultra-removal of malachite green from water,Environ.Technol.Innov. 21 (2021): 101305. https://doi.org/10.1016/j.eti.2020.101305.

[14] TA Saleh, SH Al-Ruwayshid, A Sarı, M Tuzen,Synthesis of silica nanoparticles grafted with copolymer of acrylic acrylamide for ultra-removal of methylene blue from aquatic solutions, Eur. Polym. J. 130 (2020) 109698.https://doi.org/10.1016/j.eurpolymj.2020.109698.

[15] E. Altintig, M. Onaran, A. Sarı, H. Altundag, M. Tuzen. Preparation, characterization and evaluation of bio-based magnetic activated carbon for effective adsorption of malachite green from aqueous solution. Mater.Chem. Phys. 220 (2018) 313-321.https://doi.org/10.1016/j.matchemphys.2018.05.077.

[16] T. Mustafa, A. Sarı, T.A. Saleh, Response surface optimization, kinetic and thermodynamic studies for effective removal of rhodamine B by magnetic AC/CeO_2 nanocomposite. J.Environ.Manage. 206 (2018) 170-177. https://doi.org/10.1016/j.jenvman.2017.10.016.

[17] Y.C. Wong, Y.S. Szeto, W. Cheung, G. McKay, Adsorption of acid dyes on chitosan-equilibrium isotherm analyses. Process Biochem. 39 (2004) 695-704.https://doi.org/10.1016/S0032-9592(03)00152-3.

[18] I.A.W. Tan, A.L. Ahmad, B.H. Hameed, Adsorption of basic dye on high-surface-area activated carbon prepared from coconut husk: Equilibrium, kinetic and thermodynamic studies. J. Hazard. Mater. 154 (2008) 337-346.https://doi.org/10.1016/j.jhazmat.2007.10.031.

[19] K.G. Pavithra, P. Senthil Kumar, V. Jaikumar, P. Sundar Rajan, Removal of colorants from wastewater: A review on sources and treatment strategies. J Ind Eng Chem. 75 (2019) 1-9.https://doi.org/10.1016/j.jiec.2019.02.011.

[20] E. Alventosa-deLara, S. Barredo-Damas, M.I. Alcaina-Miranda, M.I. Iborra-Clar, Ultrafiltration technology with a ceramic membrane for reactive dye removal: optimization of membrane performance. J. Hazard. Mater. 2012 (209-210) 492-500.https://doi.org/10.1016/j.jhazmat.2012.01.065.

[21] A.K. Verma, R.R. Dash, P. Bhunia, A review on chemical coagulation/flocculation technologies for removal of colour from textile wastewaters. J. Environ. Manage. 93 (2012) 154-168.https://doi.org/10.1016/j.jenvman.2011.09.012.

[22] A.L.D. da Rosa, E. Carissimi, G.L. Dotto, H. Sander, L.A. Feris, Biosorption of rhodamine B dye from dyeing stones effluents using the green microalgae Chlorella pyrenoidosa. J. Clean. Prod. 198 (2018) 1302-1310.https://doi.org/10.1016/j.jclepro.2018.07.128.

[23] A. Asghar, A.A.A. Raman, W.M.A.W. Daud, Advanced oxidation processes for in-situ production of hydrogen peroxide/hydroxyl radical for textile wastewater treatment: a review. J. Clean. Prod. 87 (2015) 826-838.https://doi.org/10.1016/j.jclepro.2014.09.010.

[24] M.Y.A. Mollah, J.A.G. Gomes, K.K. Das, D.L. Cocke, Electrochemical treatment of Orange II dye solution-Use of aluminum sacrificial electrodes and floc characterization. J. Hazard. Mater. 174 (2010) 851-858.https://doi.org/10.1016/j.jhazmat.2009.09.131.

[25] C.H. Nguyen, R.S. Juang, Efficient removal of cationic dyes from water by a combined adsorption-photocatalysis process using platinum-doped titanate nanomaterials. J Taiwan Inst Chem Eng. 99 (2019) 166-179.https://doi.org/10.1016/j.jtice.2019.03.017.

[26] G. Kyriakopoulos, I. Xiarchos, D. Doulia, Treatment of contaminated water with pesticides via adsorption. Int. J. Environ. Technol. Manag., 6 (2006) 515-524.

[27] Y. Li, Q. Du, T.Liu, X. Peng, J. Wang, J. Sun, Y. Wang, S. Wu, Z. Wang, Y. Xia, L. Xia, Comparative study of methylene blue dye adsorption onto activated carbon, graphene oxide, and carbon nanotubes. Chem. Eng. Res. Des. 91 (2013) 361-368.https://doi.org/10.1016/j.cherd.2012.07.007.

[28] R. Sahraei, Z.S. Pour, M. Ghaemy, Novel magnetic bio-sorbent hydrogel beads based on modified gum tragacanth/graphene oxide: Removal of heavy metals and dyes from water. J. Clean. Prod. 142 (2017) 2973-2984.https://doi.org/10.1016/j.jclepro.2016.10.170.

[29] S.M. Wally, A.M. El-Wakil, W.M. Abou El-Maaty, F.S. Awad, Efficient removal of Pb (II) and Hg (II) ions from aqueous solution by amine and thiol modified activated carbon. J. Saudi Chem. Soc. 25 (2021) 101296.https://doi.org/10.1016/j.jscs.2021.101296.

[30] D. Sun, X. Zhang, Y. Wu, X. Liu, Adsorption of anionic dyes from aqueous solution on fly ash. J. Hazard. Mater. 181 (2010) 335-342.https://doi.org/10.1016/j.jhazmat.2010.05.015.

[31] S. Karaca, A. Gürses, M. Açıkyıldız, M. Ejder, Adsorption of cationic dye from aqueous solutions by activated carbon. Micropor. Mesopor. Mat. 115 (2008) 376-3782.https://doi.org/10.1016/j.micromeso.2008.02.008.

[32] M.M. Mohamed, Acid dye removal: comparison of surfactant-modified mesoporous FSM-16 with activated carbon derived from rice husk. J. Colloid Interface Sci. 272 (2004) 28-34.https://doi.org/10.1016/j.jcis.2003.08.071.

[33] M.E. Mahmoud, G.M. Nabil, N.M. El-Mallah, H.I. Bassiouny, S. Kumar, T.M. Abdel-Fattah, Kinetics, isotherm, and thermodynamic studies of the adsorption of reactive red 195 A dye from water by modified Switch grass Biochar adsorbent. J Ind Eng Chem. 37 (2016) 156-167.https://doi.org/10.1016/j.jiec.2016.03.020.

[34] S. Mubarik, A. Saeed, M.M. Athar, D.M. Iqbal, Characterization and mechanism of the adsorptive removal of 2, 4, 6-trichlorophenol by biochar prepared from sugarcane baggase. J Ind Eng Chem. 33 (2016) 115-121.https://doi.org/10.1016/j.jiec.2015.09.029.

[35] M. Rafatullah, O. Sulaiman, R. Hashim, A. Ahmad, Adsorption of methylene blue on low-cost adsorbents: a review. J. Hazard. Mater. 177 (2010) 70-80.https://doi.org/10.1016/j.jhazmat.2009.12.047.

[36] T.M. Abdel-Fattah, M.E. Mahmoud, S.B. Ahmed, M.D. Huff, J.W. Lee, S. Kumar, Biochar from woody biomass for removing metal contaminants and carbon sequestration. J Ind Eng Chem. 22 (2015) 103-109.https://doi.org/10.1016/j.jiec.2014.06.030.

[37] L. Leng, X. Yuan, G. Zeng, J. Shao, X. Chen, Z. Wu, H. Wang, X. Peng, Surface characterization of rice husk bio-char produced by liquefaction and application for cationic dye (Malachite green) adsorption. Fuel. 155 (2015) 77-85.https://doi.org/10.1016/j.fuel.2015.04.019.

[38] D. Pathania, S. Sharma, P. Singh, Removal of methylene blue by adsorption onto activated carbon developed from *Ficuscaricabast*. Arab. J. Chem. 10 (2017) S1445-S1251.https://doi.org/10.1016/j.arabjc.2013.04.021.

[39] S. Fan, Y. Wang, Z. Wang, J. Tang, J. Tang, X. Li, Removal of methylene blue from aqueous solution by sewage sludge-derived biochar: Adsorption kinetics, equilibrium, thermodynamics and mechanism. J. Environ. Chem. Eng. 5 (2017) 601-611.https://doi.org/10.1016/j.jece.2016.12.019.

[40] G. Wang, S. Wang, Z. Sun, S. Zheng, Y. Xi, Structures of nonionic surfactant modified montmorillonites and their enhanced adsorption capacities towards a cationic organic dye. Appl. Clay Sci. 148 (2017) 1-10.https://doi.org/10.1016/j.clay.2017.08.001.

[41] W. Wang, G. Huang, C. An, S. Zhao, X. Chen, P. Zhang, Adsorption of anionic azo dyes from aqueous solution on cationic gemini surfactant-modified flax shives: synchrotron infrared, optimization and modeling studies. J. Clean. Prod. 172 (2018) 1986-1997.https://doi.org/10.1016/j.jclepro.2017.11.227.

[42] S.L. Hailu, B.U. Nair, M. Redi-Abshiro, I. Diaz, M. Tessema, Preparation and characterization of cationic surfactant modified zeolite adsorbent material for adsorption of organic and inorganic industrial pollutants. J. Environ. Chem. Eng. 5 (2017) 3319-3329.https://doi.org/10.1016/j.jece.2017.06.039.

[43] Y. Xiang, M. Gao, T. Shen, G. Cao, B. Zhao, S. Guo, Comparative study of three novel organo-clays modified with imidazolium-based gemini surfactant on adsorption for bromophenol blue. J. Mol. Liq. 286 (2019) 110928.https://doi.org/10.1016/j.molliq.2019.110928.

[44] M.A.M. Salleh, D.K. Mahmoud, W.A.W.A, Karim, A. Idris, Cationic and anionic dye adsorption by agricultural solid wastes: a comprehensive review. Desalination. 280 (2011) 1-13.https://doi.org/10.1016/j.desal.2011.07.019.

[45] Y. Wu, L. Zhang, C. Gao, J. Ma, X. Ma, R. Han, Adsorption of copper ions and methylene blue in a single and binary system on wheat straw. J. Chem. Eng. Data. 54 (2009) 3229-3234.https://doi.org/10.1021/je900220q.

[46] L.P. Lingamdinne, J.R. Koduru, R.R. Karri, A comprehensive review of applications of magnetic graphene oxide based nanocomposites for sustainable water purification. J. Environ. Manage. 231 (2019) 622-6234.https://doi.org/10.1016/j.jenvman.2018.10.063.

[47] R. Nasiri, N. Arsalani, Synthesis and application of 3D graphene nanocomposite for the removal of cationic dyes from aqueous solutions: response surface methodology design. J. Clean. Prod. 190 (2018) 63-71. https://doi.org/10.1016/j.jclepro.2018.04.143.

[48] S. Wang, Y. Zhou, S. Han, N. Wang, W. Yin, X. Yin, B. Gao, X. Wang, J. Wang, Carboxymethyl cellulose stabilized ZnO/biochar nanocomposites: Enhanced adsorption and inhibited photocatalytic degradation of methylene blue. Chemosphere. 197 (2018) 20-25.https://doi.org/10.1016/j.chemosphere.2018.01.022.

[49] M.M. Iqbal, M. Imran, T. Hussain, M.A. Naeem, A.A. Al-Kahtani, G.M. Shah, S. Ahmad, A. Farooq, M. Rizwan, A. Majeed, A.R. Khan, S. Ali, Effective sequestration of Congo red dye with ZnO/cotton stalks biochar nanocomposite: MODELING, reusability and stability. J. Saudi Chem. Soc. 25 (2021) 101176.https://doi.org/10.1016/j.jscs.2020.101176.

[50] J. Xie, R. Lin, Z. Liang, Z. Zhao, C. Yang, F. Cui, Effect of cations on the enhanced adsorption of cationic dye in Fe_3O_4-loaded biochar and mechanism. J. Environ. Chem. Eng. 9 (2021) 105744.https://doi.org/10.1016/j.jece.2021.105744.

[51] P. Zhang, D. O'Connor, Y. Wang, L. Jiang, T. Xia, L. Wang, D.C.W. Tsang, Y.S. Ok, D. Hou, A green biochar/iron oxide composite for methylene blue removal. J. Hazard. Mater. 384 (2020) 121286.https://doi.org/10.1016/j.jhazmat.2019.121286.

[52] Y. Bulut, H. Aydın, A kinetics and thermodynamics study of methylene blue adsorption on wheat shells. Desalination. 194 (2006) 259-267.https://doi.org/10.1016/j.desal.2005.10.032.

[53] F. Ferrero, Dye removal by low cost adsorbents: hazelnut shells in comparison with wood sawdust. J. hazard. Mater. 142 (2007) 144-152.https://doi.org/10.1016/j.jhazmat.2006.07.072.

[54] X. Wang, M.R. Bayan, M. Yu, D.K. Ludlow, X. Liang, Atomic layer deposition surface functionalized biochar for adsorption of organic pollutants: improved hydrophilia and adsorption capacity. Int J Environ Sci Technol. 14 (2017) 1825-1834.https://doi.org/10.1007/s13762-017-1300-8.

[55] A. Khataee, B. Kayan, P. Gholami, D. Kalderis, S. Akay, L. Dinpazhoh, Sonocatalytic degradation of Reactive Yellow 39 using synthesized ZrO_2 nanoparticles on biochar. UltrasonSonochem. 39 (2017) 540-549.https://doi.org/10.1016/j.ultsonch.2017.05.023.

[56] X. Cai, J. Li, Y. Liu, Z. Yan, X. Tan, S. Liu, G. Zeng, Y. Gu, X. Hu, L. Jiang, Titanium dioxide-coated biochar composites as adsorptive and photocatalytic degradation materials for the removal of aqueous organic pollutants. J. Chem. Technol. Biotechnol. 93 (2018) 783-791. https://doi.org/10.1002/jctb.5428.

[57] A, Nayak, B. Bhushan, V. Gupta, S. Kotnala, Fabrication of microwave assisted biogenic magnetite-biochar nanocomposite: A green adsorbent from jackfruit peel for

removal and recovery of nutrients in water sample. J Ind Eng Chem. 100 (2021) 134-148.https://doi.org/10.1016/j.jiec.2021.05.028.

[58] A. Buthiyappan, J. Gopalan, A.A.A. Raman, Synthesis of iron oxides impregnated green adsorbent from sugarcane bagasse: Characterization and evaluation of adsorption efficiency. J. Environ. Manage. 249 (2019) 109323.https://doi.org/10.1016/j.jenvman.2019.109323.

[59] W. Jiang, L. Zhang, X. Guo, M. Yang, Y. Lu, Y. Wang, Y. Zheng, G. Wei, Adsorption of cationic dye from water using an iron oxide/activated carbon magnetic composites prepared from sugarcane bagasse by microwave method. Environ. Technol. 42 (2021) 337-350.https://doi.org/10.1080/09593330.2019.1627425.

[60] A.K.A.N. Sadiye, Phytochemicals in avocado peel and their potential uses. Food and Health. 7 (2020) 138-149.

[61] M.P. Elizalde-González, J. Mattusch, A.A. Peláez-Cid, R. Wennrich, Characterization of adsorbent materials prepared from avocado kernel seeds: Natural, activated and carbonized forms. J Anal Appl Pyrolysis. 78 (2007) 185-193.https://doi.org/10.1016/j.jaap.2006.06.008.

[62] M. Bhaumik, H.J. Choi, M.P. Seopela, R.I. McCrindle, A. Maity, Highly effective removal of toxic Cr(VI) from wastewater using sulfuric acid-modified avocado seed. Ind. Eng. Chem. Res. 53 (2014) 1214-1224. https://doi.org/10.1021/ie402627d.

[63] H.N. Tran, S.J. You, A. Hosseini-Bandegharaei, H.-P. Chao, Mistakes and inconsistencies regarding adsorption of contaminants from aqueous solutions: a critical review. Water Res. 2017; 120: 88–116. https://doi.org/10.1016/j.watres.2017.04.014.

[64] N. Ayawei, S.S. Angaye, D. Wankasi, E.D. Dikio, Synthesis, characterization and application of Mg/Al layered double hydroxide for the degradation of congo red in aqueous solution. Open J. Phys. Chem. 5 (2015)56. doi.org/10.4236/ojpc.2015.53007.

[65] M.S. Alhumaimess, Sulfhydryl functionalized activated carbon for Pb (II) ions removal: kinetics, isotherms, and mechanism, Sep. Sci. Technol. 55 (2020) 1303-1316. ttps://doi.org/10.1080/01496395.2019.1589513.

[66] K.Y. Foo, B.H. Hameed, Insights into the modeling of adsorption isotherm systems. Chem. Eng. J. 156 (2010) 2-10.https://doi.org/10.1016/j.cej.2009.09.013.

[67] P.K. Malik, Use of activated carbons prepared from sawdust and rice-husk for sorption of acid dyes: a case study of acid yellow 36. Dyes Pigm. 56 (2003) 239–249.https://doi.org/10.1016/S0143-7208(02)00159-6.

[68] H. Shahbeig, N. Bagheri, S.A. Ghorbanian, A. Hallajisani, S. Poorkarimi, A new adsorption isotherm model of aqueous solutions on granular activated carbon. World J Modell Simul 9 (2013) 243–254.

[69] M. Benadjemia, L. Millière, L. Reinert, N. Benderdouche, L. Duclaux, Preparation, characterization and Methylene Blue adsorption of phosphoric acid activated carbons from globe artichoke leaves. Fuel Process. Technol. 92 (2011) 1203-1212.https://doi.org/10.1016/j.fuproc.2011.01.014.

[70] S.Zhang, Z.Huang, H.Wang, R.Liu, C.Cheng, Z.Guo, X. Yu, G.He, W. Fu, Separation of wolframite ore by froth flotation using a novel “crab” structure sebacoyl hydroxamic acid collector without $Pb(NO_3)_2$ activation, Powder Technol. 389 (2021) 96–103, https://doi.org/10.1016/j.powtec.2021.05.017.

[71] Z.Huang, S.Shuai,H.Wang,R.Liu,S.Zhang, C.Cheng,Y.Hu, X.Yu, G.He,W.Fu, Froth flotation separation of lepidolite ore using a new Gemini surfactant as the flotation collector,Sep. Purif. Technol. 282, (2022), 119122,https://doi.org/10.1016/j.seppur.2021.119122.

[72] M.Shkoor, H.Mehanna, A.Shabana, T.Farhat, A.D. Bani- Yaseen, Experimental and DFT/TD-DFT computational investigations of the solvent effect on the spectral properties of nitro substituted pyridine [3,4-c]coumarins, J. Mol. Liq. 313 (2020) 113509,https://doi.org/10.1016/j.molliq.2020.113509.

[73] Y.F. Shen, J. Tang, Z.H. Nie, Y.D. Wang, Y. Ren, L. Zuo, Tailoring size and structural distortion of Fe_3O_4 nanoparticles for the purification of contaminated water. Bioresour. Technol. 100 (2009) 4139-4146.https://doi.org/10.1016/j.biortech.2009.04.004.

[74] H. Khoshsang, A. Ghaffarinejad, H, Kazemi, Y. Wang, H. Arandiyan, One-pot synthesis of S-doped Fe_2O_3/C magnetic nanocomposite as an adsorbent for anionic dye removal: equilibrium and kinetic studies. J Nanostructure Chem. 8 (2018) 23-32.https://doi.org/10.1007/s40097-017-0251-4.

[75] M. Jain, M. Yadav, T. Kohout, M. Lahtinen, V.K. Garg, M. Sillanpää, Development of iron oxide/activated carbon nanoparticle composite for the removal of Cr (VI), Cu (II) and Cd(II) ions from aqueous solution. Water Resour. Ind. 20 (2018) 54-74.https://doi.org/10.1016/j.wri.2018.10.001.

[76] A.M. Dehkhoda, N. Ellis, E. Gyenge, Electrosorption on activated biochar: effect of thermo-chemical activation treatment on the electric double layer capacitance. J Appl Electrochem. 44 (2014) 141-157. DOI 10.1007/s10800-013-0616-4.

[77] K. Sun, K. Ro, M. Guo, J. Novak, H. Mashayekhi, B. Xing, Sorption of bisphenol A, 17α-ethinyl estradiol and phenanthrene on thermally and hydrothermally produced biochars. Bioresour. Technol. 102 (2011) 5757-5763.https://doi.org/10.1016/j.biortech.2011.03.038.

[78] J. Chen, J. Qiu, B. Wang, H. Feng, K. Ito, E. Sakai, Fe_3O_4/biocarbon composites with superior performance in supercapacitors. J. Electroanal. Chem. 804 (2017) 232-239.https://doi.org/10.1016/j.jelechem.2017.09.028.

[79] H. Cui, D. Li, Z. Zhang, Preparation and characterization of Fe_3O_4 magnetic nanoparticles modified by perfluoropolyether carboxylic acid surfactant, Mater. Lett. 143 (2015) 38–40. https://doi.org/10.1016/j.matlet.2014.12.037.

[80] A.E. Pirbazari, E. Saberikhah, S.S.H. Kozani, Fe_3O_4–wheat straw: preparation, characterization and its application for methylene blue adsorption, Water Resour. Ind. 7-8 (2014) 23–37. https://doi.org/10.1016/j.wri.2014.09.001.

[81] Y. Yu, C. Ouyang, Y. Gao, Z. Si, W. Chen, Z. Wang, G. Xue, Synthesis and characterization of carbon nanotube/polypyrrole core–shell nanocomposites via in situ inverse microemulsion. J. Polym. Sci. A Polym. Chem. 43 (2005) 6105-6115. https://doi.org/10.1002/pola.21114.

[82] R.M. Suzuki, A.D. Andrade, J.C. Sousa, M.C. Rollemberg, Preparation and characterization of activated carbon from rice bran. Bioresour. Technol. 98 (2007) 1985-1991.https://doi.org/10.1016/j.biortech.2006.08.001.

[83] W. Chen, X. Rong, J. Peng, Q. Tang, H. Luo, L. Fan, K. Feng, H. Zheng, Assessment of a novel nanostructured flocculant with elevated flocculation and

antimicrobial activity. Chemosphere. 239 (2020) 124736.https://doi.org/10.1016/j.chemosphere.2019.124736.

[84] Y. An, H. Zheng, Z. Yu, Y. Sun, Y. Wang, C. Zhao, W. Ding, Functioned hollow glass microsphere as a self-floating adsorbent: Rapid and high-efficient removal of anionic dye. J. Hazard Mater. 381 (2020) 120971.https://doi.org/10.1016/j.jhazmat.2019.120971.

[85] X. Zheng, H. Zheng, Z. Xiong, R. Zhao, Y. Liu, C. Zhao, C. Zheng, Novel anionic polyacrylamide-modify-chitosan magnetic composite nanoparticles with excellent adsorption capacity for cationic dyes and pH-independent adsorption capability for metal ions. Chem. Eng. J. 392 (2020) 123706.https://doi.org/10.1016/j.cej.2019.123706.

[86] Y. Li, A.R. Zimmerman, F. He, J. Chen, L. Han, H. Chen, X. Hu, B. Gao, Solvent-free synthesis of magnetic biochar and activated carbon through ball-mill extrusion with Fe_3O_4 nanoparticles for enhancing adsorption of methylene blue. Sci. Total Environ. 722 (2020) 137972.https://doi.org/10.1016/j.scitotenv.2020.137972.

[87] Y.C. Sharma, Optimization of parameters for adsorption of methylene blue on a low-cost activated carbon. J. Chem. Eng. Data. 2010; 55(1):435-439.https://doi.org/10.1021/je900408s.

[88] N. Ballav, S. Debnath, K. Pillay, A. Maity, Efficient removal of Reactive Black from aqueous solution using polyaniline coated ligno-cellulose composite as a potential adsorbent. J. Mol. Liq. 209 (2015) 387-396.https://doi.org/10.1016/j.molliq.2015.05.051.

[89] N. Barka, S, Qourzal, A. Assabbane, A. Nounah, Y. Ait-Ichou, Removal of reactive yellow 84 from aqueous solutions by adsorption onto hydroxyapatite. J. Saudi Chem. Soc. 15 (2011) 263-267.

[90] S. Chatterjee, T. Chatterjee, S.R. Lim, S.H. Woo, Adsorption of a cationic dye, methylene blue, on to chitosan hydrogel beads generated by anionic surfactant gelation. Environ. Technol. 32 (2011) 1503-1514.https://doi.org/10.1080/09593330.2010.543157.

[91] Z. Zhang, S. Xia, X. Wang, A. Yang, B. Xu, L. Chen, Z. Zhu, J. Zhao, N. Jaffrezic-Renault, D.Leonard, A novel biosorbent for dye removal: extracellular polymeric substance (EPS) of Proteus mirabilis TJ-1. J. Hazard. Mater. 2009; 163(1):279-284.https://doi.org/10.1016/j.jhazmat.2008.06.096.

[92] C. Chen, S. Mi, D. Lao, P. Shi, Z. Tong, Z. Li, H. Hu, Single-step synthesis of eucalyptus sawdust magnetic activated carbon and its adsorption behavior for methylene blue. RSC adv. 9 (2019) 22248-22262.DOI: 10.1039/C9RA03490K.

[93] M.M. Abd El-Latif, A.M. Ibrahim, Adsorption, kinetic and equilibrium studies on removal of basic dye from aqueous solutions using hydrolyzed oak sawdust. Desalin. water Treat. 6 (2009) 252-268.

[94] O. Duman, S. Tunç, T.G. Polat, B.K. Bozoğlan, Synthesis of magnetic oxidized multiwalled carbon nanotube-κ-carrageenan-Fe_3O_4 nanocomposite adsorbent and its application in cationic Methylene Blue dye adsorption. Carbohydr. Polym. 147 (2016) 79-88.https://doi.org/10.1016/j.carbpol.2016.03.099.

[95] A. El Nemr,O.Abdelwahab, A. El-Sikaily, A. Khaled, Removal of direct blue-86 from aqueous solution by new activated carbon developed from orange peel. J. Hazard.Mater. 161 (2009) 102-110.https://doi.org/10.1016/j.jhazmat.2008.03.060.

[96] K.L. Tan, B.H. Hameed, Insight into the adsorption kinetics models for the removal of contaminants from aqueous solutions. J.Taiwan Inst. Chem. Eng. 74 (2017) 25-48.https://doi.org/10.1016/j.jtice.2017.01.024.

[97] B. van Veenhuyzen, S. Tichapondwa, C. Hörstmann, E. Chirwa, H.G. Brink, High capacity Pb(II) adsorption characteristics onto raw-and chemically activated waste activated sludge. J. Hazard. Mater. 416 (2021) 125943.https://doi.org/10.1016/j.jhazmat.2021.125943.

[98] K.G. Bhattacharyya, A. Sharma, Kinetics and thermodynamics of methylene blue adsorption on neem (Azadirachtaindica) leaf powder. DyesPigm. 65 (2005) 51-59.https://doi.org/10.1016/j.dyepig.2004.06.016.

[99] Z. Wang, J. Zhao, L. Song, H. Mashayekhi, B. Chefetz, B. Xing, Adsorption and desorption of phenanthrene on carbon nanotubes in simulated gastrointestinal fluids. Environ. Sci. Technol. 45 (2011) 6018–6024.https://doi.org/10.1021/es200790x.

[100] O, Duman, T.G. Polat, C.O. Diker, S. Tunc, Agar/kappa-carrageenan composite hydrogel adsorbent for the removal of Methylene Blue from water, Int. J. Biol. Macromol. 160 (2020) 823-835.https://doi.org/10.1016/j.ijbiomac.2020.05.191.

[101] C.P. Pinheiro, L.M.K. Moreira, S.S. Alves, T.R.S. Cadaval Jr, L.A.A. Pinto, Anthocyanins concentration by adsorption onto chitosan and alginate beads: Isotherms, kinetics and thermodynamics parameters. Int. J. Biol. Macromol. 166 (2021) 934-939.

[102] A. Bhatnagar, Y.H. Choi, Y.J. Yoon, Y. Shin, B.-H. Jeon, J.-W. Kang, Bromate removal from water by granular ferric hydroxide (GFH). J. Hazard. Mater. 170 (2009) 134-140.https://doi.org/10.1016/j.jhazmat.2009.04.123.

[103] Y. Yoon, M. Zheng, Y.-T. Ahn, W.K. Park, W.S. Yang, J.-W. Kang, Synthesis of magnetite/non-oxidative graphene composites and their application for arsenic removal. Sep. Purif. Technol. 178 (2017) 40-48. https://doi.org/10.1016/j.seppur.2017.01.025.

[104] W.J. Weber Jr, J.C. Morris, Kinetics of adsorption on carbon from solution, J. Sanit. Eng. Div. Am. Soc. Civil Eng. 89 (1963) 31–59. https://doi.org/10.1061/JSEDAI.0000430.

[105] F. Deng, J. Liang, G. Yang, X. Hu, Q. Huang, J. Dou, Y. Wen, M. Liu, X. Zhang, Y. Wei. Gamma-ray initiated polymerization from polydopamine-modified MoS_2 nanosheets with poly (ionic liquid) and their utilization for adsorptive organic dyes with enhanced efficiency. CEJ Advances 7 (2021) 100134.https://doi.org/10.1016/j.ceja.2021.100134.

[106] C. Zheng, H. Zheng, C. Hu, Y. Wang, Y. Wang, C. Zhao, W. Ding, Q. Sun, Structural design of magnetic biosorbents for the removal of ciprofloxacin from water. Bioresour. Technol. 2020: 296:122288. https://doi.org/10.1016/j.biortech.2019.122288.

[107] G.Yang, Q. Huang, D. Gan, H. Huang, J. Chen, F. Deng, M. Liu, Y. Wen, X. Zhang, Y. Wei, Biomimetic functionalization of carbon nanotubes with poly (ionic liquids) for highly efficient adsorption of organic dyes. J. Mol. Liq. 2019; 296: 112059.https://doi.org/10.1016/j.molliq.2019.112059.

[108] A.A. Inyinbor, F.A. Adekola, G.A. Olatunji, Kinetics, isotherms and thermodynamic modeling of liquid phase adsorption of Rhodamine B dye onto Raphia hookerie fruit epicarp. Water Resour. Ind. 15 (2016) 14-27. https://doi.org/10.1016/j.wri.2016.06.001.

[109] Y. Jiang, Q. Mao, T. Ma, X. Liu, Y. Li, S. Ren, J. Sun. Facile preparation of Fe_2O_3 Al_2O_3 composite with excellent adsorption properties towards Congo red. Ceram. Int. 47 (2021) 13884-13894.https://doi.org/10.1016/j.ceramint.2021.01.255.

[110] E.S. Pouya, H. Abolghasemi, M. Esmaieli, H. Fatoorehchi, S.J. Hashemi, A. Salehpour, Batch adsorptive removal of benzoic acid from aqueous solution onto modified natural vermiculite: Kinetic, isotherm and thermodynamic studies. J Ind Eng Chem. 31 (2015) 199-215.https://doi.org/10.1016/j.jiec.2015.06.024.

[111] T.L. Silva, A.L. Cazetta, P.S.C. Souza, T. Zhang, T. Asefa, V.C. Almeida, Mesoporous activated carbon fibers synthesized from denim fabric waste: efficient adsorbents for removal of textile dye from aqueous solutions. J. Clean. Prod. 171 (2018) 482-490.https://doi.org/10.1016/j.jclepro.2017.10.034.

[112] N. Djebri, N. Boukhalfa, M. Boutahala, D. Hauchard, N.E. Chelali, A. Kahoul, Calcium alginate-organobentonite-activated carbon composite beads as a highly effective adsorbent for bisphenol A and 2, 4, 5-trichlorophenol: kinetics and equilibrium studies. Desalin. Water Treat. 83 (2017) 294-305.DOI:10.5004/dwt.2017.20873.

[113] Y. Liu, Y.J. Liu, Biosorption isotherms, kinetics and thermodynamics. Sep. Purif. Technol. 61 (2008) 229-242.https://doi.org/10.1016/j.seppur.2007.10.002.

[114] M.M. Kamel, I.H. Alsohaimi, M.S. Alhumaimess, H.M.A. Hassan, M.S. Alshammari, M.Y. El-Sayed, A glassy polyvinyl alcohol/silica gel hybrid composite for safranin removal: Adsorption, kinetic and thermodynamic studies. Res. Chem. Intermed.47 (2021) 925-944.https://doi.org/10.1007/s11164-020-04309-2.

[115] H.Y. Zhu, R. Jiang, L. Xiao, G.M. Zeng, Preparation, characterization, adsorption kinetics and thermodynamics of novel magnetic chitosan enwrapping nanosized γ-Fe_2O_3 and multi-walled carbon nanotubes with enhanced adsorption properties for methyl orange. Bioresour. Technol. 101 (2010) 5063-5069. https://doi.org/10.1016/j.biortech.2010.01.107.

[116] Y. Liu, Q. Gao, C. Li, S. Liu, K. Xia, B. Han, C. Zhou, Effective coating of cross linked polyethyleneimine on elastic spongy monolith for highly efficient batch and continuous flow adsorption of Pb (II) and acidic red 18. Chem. Eng. J. 391 (2020) 123610. https://doi.org/10.1016/j.cej.2019.123610.